STUDIES OF CERAMIC PROCESSING (U)

FINAL REPORT

December 1, 1964, to December 15, 1965

by
F. L. Fleischner
C. M. Ringel
E. J. Smoke

Prepared under Contract NOw 65–0199–d for the
U.S. Navy, Bureau of Weapons

by the

School of Ceramics

Rutgers, The State University

New Brunswick, New Jersey

Distribution of this document is unlimited.

STUDIES OF CERAMIC PROCESSING

E. J. Smoke, C. M. Ringel and P. L. Fleischner

School of Ceramics

RUTGERS · THE STATE UNIVERSITY

Abstract

The objective of this program is to improve the structure of ceramics by processing. The over-all temperature range of interest is 1800 to above 3000°F. In the high portion of the range, 3000°F and above, compositions of pure alumina plus 0 to 2% additions of MgO were studied between 2822 and 3180°F, at 1 to 7 hour soaking periods and in atmospheres of hydrogen, helium and vacuum. This work was reported in the previous Final Report; however, the analysis of results is reported herein. Petrographic, x-ray, d.c. conductivity, electron transmission and electron probe methods were used and the results are reported. The second temperature range, 2600-3000°F, was studied utilizing the presintered approach to the prereacted raw materials technique and the results were reported in earlier reports. The low range, 1800 to 2600°F, was studied using the devitrification approach to the prereacted materials technique. The area of crystallization of cordierite in the $MgO \cdot Al_2O_3 \cdot SiO_2$ system was evaluated as a single glass system. A two-glass system, in which one glass devitrifies cordierite and the second supplies the bonding system, was studied. Bonding glass compositions were evaluated in the $RO \cdot Al_2O_3 \cdot SiO_2$ system, in which the RO members are alkaline earth oxides. Composites were made at 10, 20 and 30% bonding glass. Processing, structures and properties are reported.

TABLE OF CONTENTS

LIST OF TABLES

LIST OF ILLUSTRATIONS

LIST OF ILLUSTRATIONS (continued)

I. Introduction

This research program is directed toward a study of materials and processes by which ceramics suitable for radome applications can be processed at temperatures considerably lower than their maximum use temperature. The basis for the effort reported herein was established under Contract NOw-64-0040-d. The temperature range that can be studied is from the melting temperature of the most refractory crystalline phases showing promise of meeting the prime requirements to as low as 1800°F.

The over-all temperature range has been divided into three narrower ranges: 3000°F and above, 2600 to 3000°F, and 1800 to 2600°F. In the highest range, a sintering study of pure alumina is being conducted with respect to the processing parameters and sintering mechanisms by which the objectives can be accomplished. In the 2600 to 3000°F temperature range, the most promising approach is the prereacted raw materials technique using high alumina compositions. This area has been studied extensively and is reported in previous contracts. In the lowest temperature range, 1800 to 2600°F, the "two-glass system" of the devitrification approach to the prereacted raw materials technique is being studied. In this method two compositions are prepared and mixed separately on an atomic basis by melting and fritting. These frits are mixed in specific ratios, then ground to a controlled particle size distribution conducive for processing by conventional ceramic processes such as casting, pressing, etc. During firing one frit devitrifies to form the principal crystalline phase, while the second promotes sintering and supplies the bond. Some frits used in this latter manner have been designed to devitrify after performing the sintering and bonding functions. Cordierite, $2MgO \cdot 2Al_2O_3 \cdot 5SiO_2$, is the crystalline phase presently under investigation and is supplied by the first frit. The second glass is of the alkaline earth (BaO, MgO, CaO) aluminosilicate type.

The processing parameters, for realizing the objectives of the project in the highest temperature range, were established under Contract NOw-64-0040-d. A study of the sintering mechanisms by which this was accomplished comprises the first phase of this Final Report, along with a summary and discussion of the role of the processing parameters. The second phase is a study of the two-glass system of the devitrification approach of the prereacted raw materials technique which is designed to function in the 1800-2600°F temperature range.

II. Sintering Studies

A. Introduction

In the highest temperature range, namely 3000°F and above, the effort of this continuing program has been devoted to determining the parameters and mechanisms by which pure alumina can be sintered to 99+% of its true density, with particular emphasis on lowering firing temperature yet retaining all engineering properties, including refractoriness. The sintering characteristics of pure alumina plus 0 to 2% magnesia have been studied as a function of temperature and time when fired in helium, oxygen and vacuum respectively. The parameters have been determined for attaining theoretical density; 99% has been attained at as low as 2822°F (1550°C). The present objective is to attempt to determine the mechanisms responsible for this. The primary one is to determine the function of magnesia in promoting sintering and inhibiting crystal growth. One approach

was to attempt to determine the distribution of magnesia and whether it was in solid solution with alumina. The back-reflection x-ray ceramic technique was utilized along with the electron probe. This latter tool determined the distribution and concentration of both magnesium and aluminum. Defects are considered an important driving force for sintering. Transmission electron microscopy was used in an attempt to determine the quenched defect structure associated with sintering in this system. Determination of activation energies associated with the sintering process and the role of the variables of this study was attempted using porosity data and electrical measurements.

B. Review of Parameters Essential for the Sintering of the Alumina Compositions Studied

A brief review of the compositions, procedure, including firing, and results is pertinent to an understanding of the results of the attempts to determine the mechanisms operative in attaining high density in these compositions. This information is described in detail in the Final Report of Contract NOw-64-0040-d.

Three compositions were chosen for intensive study: Composition C is 100% alumina; Composition R is 99.75% alumina, 0.25% magnesia; and Composition CR is 98.0% alumina and 2.0% magnesia. Both raw materials are 99.99% pure. The function of the magnesia is to minimize grain growth. The mechanism may be solid solution; however, this remains to be proven. The compositions were wet-mixed and specimens fabricated by dry pressing. Air as a firing atmosphere is not conducive to attaining a high percentage of true density. Considerable work is reported on firing in various atmospheres; however, the conditions vary appreciably. Hydrogen, helium and vacuum were selected for study. The first two were chosen because they can diffuse quite readily. Further, hydrogen is an active gas and is a reducing agent which can produce defects; also, it may diffuse as H°, H^{+} and possibly as H_2. Helium is an inert gas and its small size and its high diffusion rate are its prime assets. Vacuum will reduce the gas pressure within the pores and maximize gas diffusion from the structure. All compositions were fired for 1, 3, 5 and 7 hours respectively at 1550, 1650, 1700 and 1750°C respectively. A special molybdenum resistance furnace was used for all fires.

Percent total porosity was measured by bulk density measurements and augmented petrographically in the lowest porosity region.

Figure 1 shows the effect of firing time on percent total porosity of all three compositions fired in hydrogen, helium and vacuum over the time-temperature range noted above. The objective is the lowest firing temperature at which 99% of true density, or less than 1% porosity, is attained. This is attained by firing in vacuum to 1550°C (2822°F) after a three-hour soaking period with the CR composition (2% MgO), and after 7 hours with the R composition (1/4% MgO). It can also be attained by firing in hydrogen to 1650°C (3000°F) after a one-hour soaking period with either of the compositions containing magnesia. Further, it can be realized by firing to the same temperature in helium but only after approximately a four-hour soak. To approach true density or total porosity less than 0.1% it is necessary to fire to 1750°C in either vacuum or hydrogen. The R composition (1/4% MgO) attains the quality at one-hour soak in either atmosphere. The CR composition (2% MgO) must be fired approximately 3 hours to reach this quality. The percent total pore volume of the pure alumina composition reaches a minimum of 1.9% at the highest temperature, but only in a vacuum. The

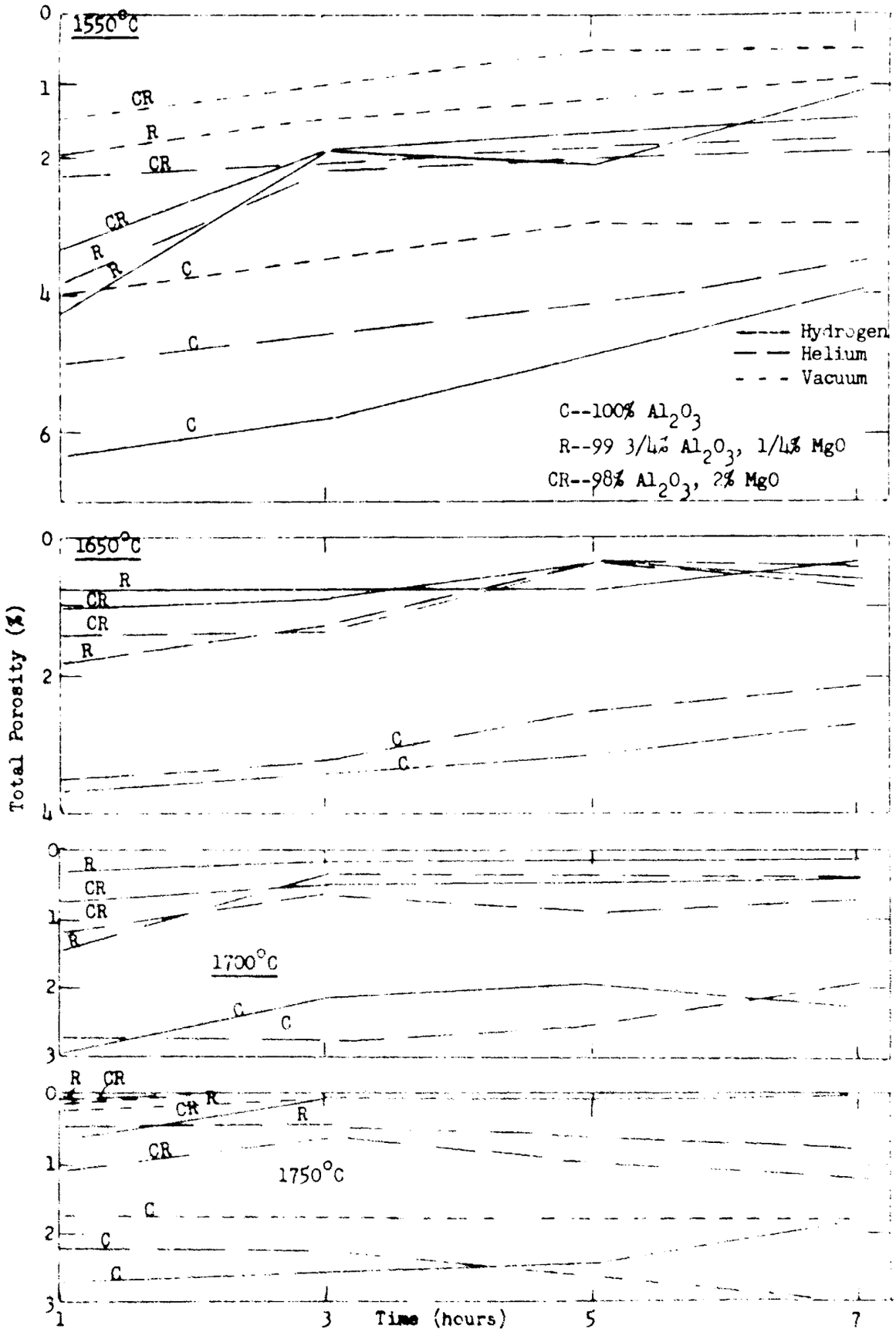

Fig. 1--Porosity vs. Firing Temperature, Time and Atmosphere

reason for this is the exaggerated grain growth exhibited by this composition. The magnesia included in the R and CR compositions acts as a grain growth inhibitor. Further, it results in a higher sintering rate; the postulated reason is that it is due to solid solution with alumina creating a greater concentration of vacancies. Figure 2 shows that the maximum average crystal size developed in either of the magnesia-containing compositions is 18 microns, while that of the pure alumina at the highest temperature is 35 microns. Spinel formation is detected in both magnesia-containing compositions.

Thus the lowest temperature at which a nearly pure alumina composition can attain less than 1% total pore volume is 1550°C (2822°F). This is accomplished using 2% magnesia as a grain growth inhibitor and firing in a vacuum for 3 hours. At 1/4% magnesia this quality is reached only after 7 hours' soak. A hydrogen atmosphere necessitates an increase in firing temperature to 1650°C (3000°F) and soaking for 1 hour, while when firing in helium the soaking period must be increased to 4 hours; this holds for both magnesia-containing compositions. The total pore volume of the pure alumina composition never gets below 1.9% even at the highest temperature and soaking periods.

C. Study of Sintering Mechanisms

1. General

In attempting to determine the sintering mechanisms effective in this study of alumina with additions of 0 to 2% magnesia, two approaches were used. The first was to attempt to determine the role of "vacancy movement" and "defect structure." These are considered important structural conditions which promote sintering. Electrical measurements were used for the former while electron transmission methods were used to attempt to measure the latter. The second approach was to attempt to determine the mechanisms by which magnesia promotes sintering and inhibits grain growth. These two approaches are undoubtedly interrelated as the presence of the magnesia may cause vacancies and defects.

2. Activation Energy for Vacancy Movement

In order to understand the role magnesia plays in sintering, an attempt was made to determine the activation energy of vacancy movement in compositions with and without magnesia additions. When electrical measurements of the composition are made in the d.c. conductivity region, activation energies for vacancy movement can be determined (Refs. 1-4).

The region of d.c. conductivity for most ionic crystals occurs when using direct current, or alternating current of very low frequencies, i.e., 1 cycle/sec. When d.c. conductivity predominates in ionic crystals, conduction occurs by vacancy movement. The following equation is used for d.c. conductivity measurements:

$$\ln \tan\delta \propto \ln\sigma = \frac{\ln \nu N Q^2 A^2}{k} - \ln T - \mu/kT \qquad (1)$$

where $\tan\delta$ = dissipation factor
ν = vibrational frequency of ions
σ = conductivity
N = number of current-carrying defects/volume

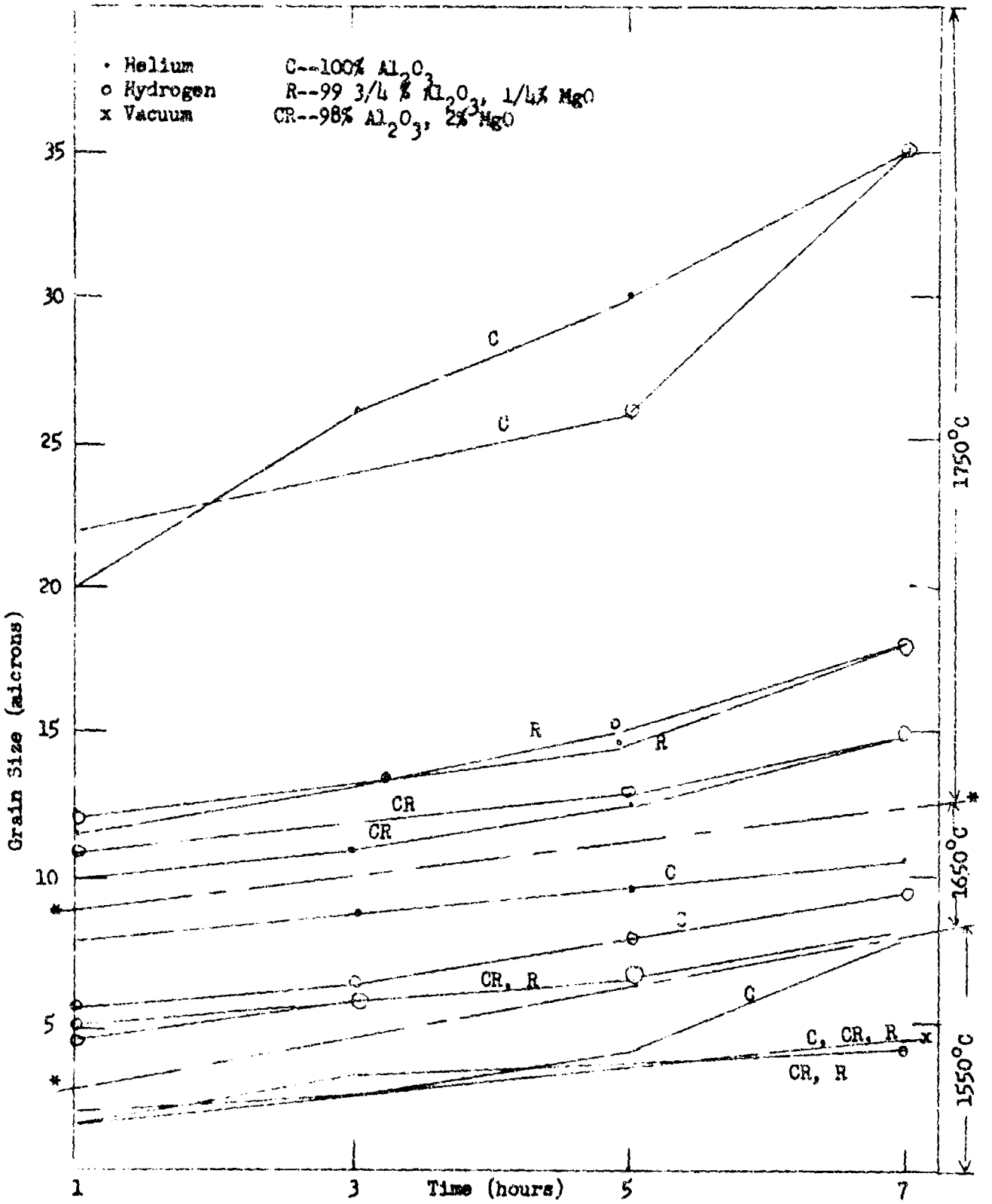

Fig. 2--Grain Size vs. Firing Temperature, Time and Atmosphere

Q = charge
A = distance defect must move to overcome energy barrier
k = Boltzman's constant
μ = activation energy for vacancy movement
T = absolute temperature

If a graph of ln tanδ vs. ln frequency is made in this region, a straight line with a unit negative slope results. This can be obtained from the relationship:

$$\tan\delta = \frac{1}{CRW} \qquad (2)$$

where C = capacitance
R = resistance
W = frequency

If a graph of ln tanδ vs. the reciprocal of the absolute temperature is plotted at a frequency in the d.c. conductivity range, the activation energy for vacancy movement can be calculated. As seen from Eq. (1), this calculation of activation energy must assume that the number of vacancies does not vary in an exponential fashion. Such variation would be the case in the pure alumina composition where the number of vacancies is governed by entropy considerations. If magnesia goes into solid solution with alumina and forms vacancies due to stoichiometry, the activation energy for vacancy movement could possibly be determined.

Samples examined were first coated with aluminum electrodes by vacuum evaporation. They contained some magnesia for the reasons given previously. They were put in a desiccator prior to test to prevent water attack. The following equipment was used in this investigation:

1) a very low frequency device for measuring tanδ and dielectric constants from .1 cps to 10 cps.[5-7]

2) 1620 A General Radio capacitance bridge, 60 cps--10 kcps.

Measurements of tanδ were made in the frequency range of 0.7 to 10 cps on a sample that contained 1/2% magnesia and was fired to 1750°C for 5 hours. If d.c. conductivity predominates, a plot of ln tanδ vs. ln frequency would result in a straight line with a slope of minus one. The data obtained for this sample is shown in Fig. 3. The range of frequency between 10 and 100 cps was not investigated because the very low frequency apparatus designed by Stevels (Refs. 1-3) will not go into this range and the jig for the other apparatus has too many losses. The results indicate that pure d.c. conductivity is not present at room temperature and in the frequency range measured with this sample. It appears from these figures that a relaxation effect occurs in this frequency range. If the temperature were increased, it might be possible to obtain d.c. conductivity data. Generally, as the temperature increases, the curve of tanδ vs. frequency is shifted to higher frequencies. If measurements were made in the same frequency range evaluated above but at increased temperatures, a shift in the relaxation curve may occur and pure d.c. conductivity might be realized. Further, since Eq. (1) is only applicable in the d.c. conductivity region, no attempt was made to plot ln tanδ vs. the reciprocal of the absolute temperature.

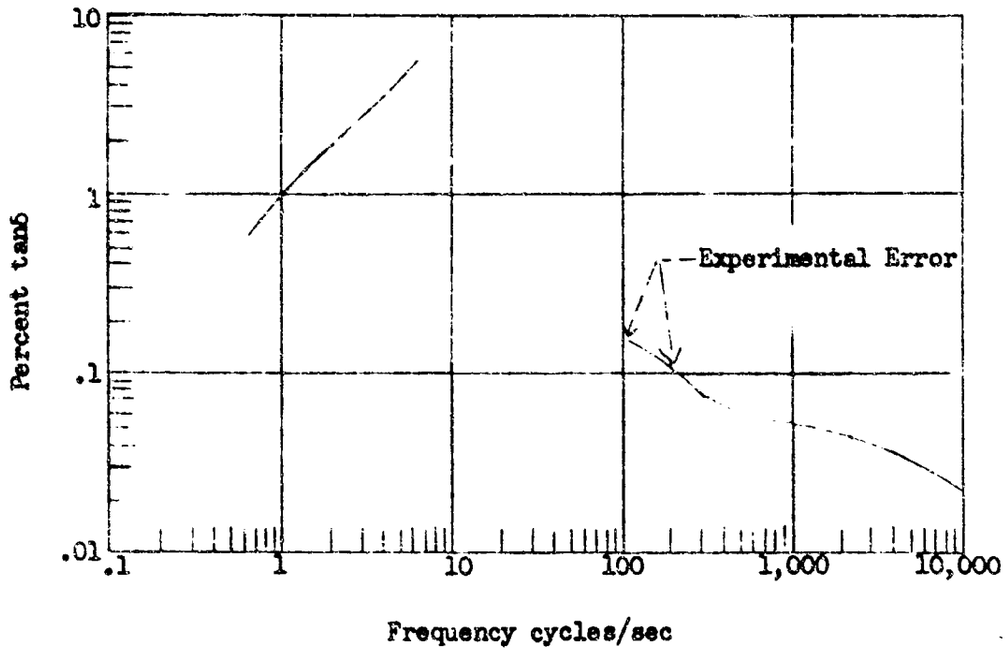

Fig. 3--Tanδ vs. Frequency for Composition R57

The literature on electrical conductivity of alumina indicates that conduction, at least at higher temperatures, is due to P-type carriers (Refs. 8, 9-11). If the temperature of this system is raised, semi-conduction behavior may be expected to interact with the d.c. conductivity.

3. Defect Structure

a. General

The primary use of the electron microscope in the field of ceramics has been in surface studies when using the replica technique (Refs. 12-16). Recently this instrument was found extremely valuable for the direct determination of defect structure (Refs. 17-22). When the electron microscope is used in transmission through a thin sample, both defect structure and crystal structure of extremely small areas can be determined. Most of the work using this technique has been devoted to metals (Refs. 19-23) and there has been little work done with ceramics; however, some published work on single crystal aluminum oxide and magnesium oxide has recently appeared (Refs. 18, 20).

Electron transmission microscopy was used as a tool to determine the sintered defect structure of some of the compositions at near theoretical density. Quenched samples were used in this method to examine the defects associated with the sintered samples at or near their sintering temperatures. It was anticipated that this study would show the following:

1) nature and types of defects produced
2) concentration gradient of the line defects found through the grain
3) some correlation of defects to sintering variables, including temperature and time at temperature, composition, etc.

The types of dislocation, their Burgers vectors, and other defects can be observed by using the tilt mechanism built into the electron microscope; by tilting the specimen, dislocation intensities either increase or decrease. The type of dislocation can be determined when the angle of tilt is known. Under the high magnification used, the study consisted of the examination of the defects associated with individual grains even though the samples were polycrystalline. A number of grains were examined to obtain a general picture of the defect structure.

The major difficulty in this method is sample preparation. To obtain an image of the structure using transmission electron microscopy the sample must be approximately 1000 Å thick. In order to be able to examine the defect structure, the variation in thickness of a specimen must be gradual as observed under the electron microscope. Electron diffraction was used in conjunction with the transmission work to determine the structure of the grain being examined.

The samples examined with this technique were within 98 to 100% of theoretical density. The reason for such a choice is that porous samples will tend to disintegrate when thinned by chemical means. The composition examined by this technique was the 2% MgO-containing composition which was sintered at the highest temperatures. Sample preparation is extremely critical. The actual examination of the prepared specimens under the electron microscope can be made only if the samples are thinned properly. The samples used must be thinned fairly uniformly to about 0.1 micron. This thinning process in metals uses an electrolytic type

of thinning apparatus in which the electrodes are first brought close to the metal and then brought further away. This results in the formation of a hole in the middle of the specimen, leaving the area surrounding the hole thin enough to be examined under the electron microscope. Another method was shown by Drum, who used sputtering to thin alumina (Ref. 23), but the samples obtained were badly damaged.

The problem of specimen preparation of ceramic materials can be divided into a number of factors:

1) finding the proper chemical thinning agent for the samples
2) finding the correct temperature and time necessary for thinning with this agent
3) avoiding etching of the sample
4) proper design of the thinning apparatus to keep the sample in continual contact with fresh thinning solution.

b. Procedure

The major problem was to prepare specimens sufficiently thin for examination under the electron microscope. Initial tests were made to determine the time, temperature, polishing or thinning agent and concentration needed to thin polycrystalline alumina samples. The first attempt at thinning alumina was done with samples of Lucalox, a General Electric Company product, and with four possible thinning agents. They were: NaOH, HCl, H_3PO_4 and NH_4OH. Three different levels of concentration were made of each: 10 molar, 1 molar and 0.1 molar. A sample of Lucalox was placed in each solution and the weight change measured. The first measurements were made at room temperature with samples held in solution for 3, 5 and 24 hours. No change in weight was noted under all conditions. By placing these solutions in a stirred constant temperature oil bath, samples could be subjected to the same treatment at elevated temperatures. The time was varied from 1 to 5 hours and the temperature raised to 70°C. No change in weight was found. A temperature of 100°C was tried next. Again no weight change was found. It was felt that these possible chemical thinning agents were not effective at these temperatures.

After examining the literature on chemical polishing of single crystal aluminum oxide, it was found that phosphoric acid in the temperature region of 400-500°C would polish alumina (Refs. 17, 18, 20, 24-27). A number of runs were made at 395°C to 430°C with Lucalox samples. It was found that both holding time and agitation of the solution surrounding the specimen were very critical. If the sample was held for too long a period of time in solution, a phosphate precipitate would form on the surface of the specimen. At temperatures between 405 and 410°C, if the sample was held in solution for short periods of time, the specimen lost weight. When these samples were observed both visually and under the microscope, it appeared that etching had taken place. Etching may be deleterious for electron transmission microscopy, since the material must be thinned fairly uniformly.

It was felt that some of the sintered samples should be investigated. Thin sections were used to minimize the thinning process and yet, because they were fairly thick, 30 microns compared to 0.1 micron needed for transmission, very few mechanical defects would be introduced to the final specimen. Samples of these thin sections were heated with phosphoric acid in a platinum crucible and

then suspended in a platinum mesh screen to 405°C. The samples were held at this temperature for 3 minutes. They were then examined under the electron microscope and found to be too thick. The specimens were again subjected to the same treatment and reexamined. After a number of tries it was found that an electron diffraction pattern could be obtained from the edges of some specimens, but it was not thin enough for transmission. In addition, there was a random distribution of samples whose edges were sufficiently thin. What occurred was that sample edges were being thinned and removed faster than its depth. Therefore, if the sample was removed at the proper time, perhaps an edge would be present, but this was a random factor.

In order to avoid the above problem, it was decided that an indentation should be drilled into the thin section, using an ultrasonic drill. In this way the material within the indentation would be thinned preferentially or at the same rate as the bulk. A hole should form in the center of the specimen, while the sample maintained its original shape and structure. The area around this hole should be sufficiently thin for electron transmission. A few runs were attempted using this geometry, but the samples were coated with a phosphate precipitate which interfered with the polishing. This compound formed from solution during the thinning operation.

In order to eliminate the contamination problem, a jet thinning device was used as noted in Fig. 4 (Ref. 18). The design of this device is based on the fact that during heating the boiling point of phosphoric acid is raised as the acid condenses. With rapid heating, boiling action can be maintained up to temperatures of about 520°C. The device is made of platinum and is similar to a coffee maker in design. The inventor of the device used it to prepare single crystal alumina for electron transmission microscopy studies. Since boiling action forces the liquid up through a small tube and hits the specimens and then drops off, the specimen is in continual contact with uncontaminated solution. Therefore, thinning can proceed without phosphate build-up. The inventor found that the polishing temperature was about 50°C higher than the etching temperature for alumina single crystals.

The jet thinning device was placed in a small nicrome-wound furnace. Five cubic centimeters of orthophosphoric acid were added to the device. The thinning apparatus was heated at a rate of 400°C/12 minutes. This rate was necessary to maintain boiling action through the central pump tube at 450°C. Temperatures were measured with a chromel-alumel thermocouple. Four tenths of a cubic centimeter of fresh phosphoric acid were added at 192, 215 and 245°C respectively; one cubic centimeter was then added at 350°C. The sample was placed in a specimen stand, lowered and made to rest just above the central pump tube at 425°C. Runs were made from 1/2-3 minutes at temperatures between 450 and 475°C. Fresh acid was added to lower the rate of temperature rise and to maintain boiling action through the pump tube in this temperature range. An attempt was made to view the sample under a 40x Bausch and Lomb microscope, but wetting of the specimen stand occurred and direct observations could not be made. Since the indentation made was of varying thickness, no exact holding time could be predicted. Generally, the holding time varied from about 1 to 3 minutes and samples with holes about 10-50 microns in diameter were formed.

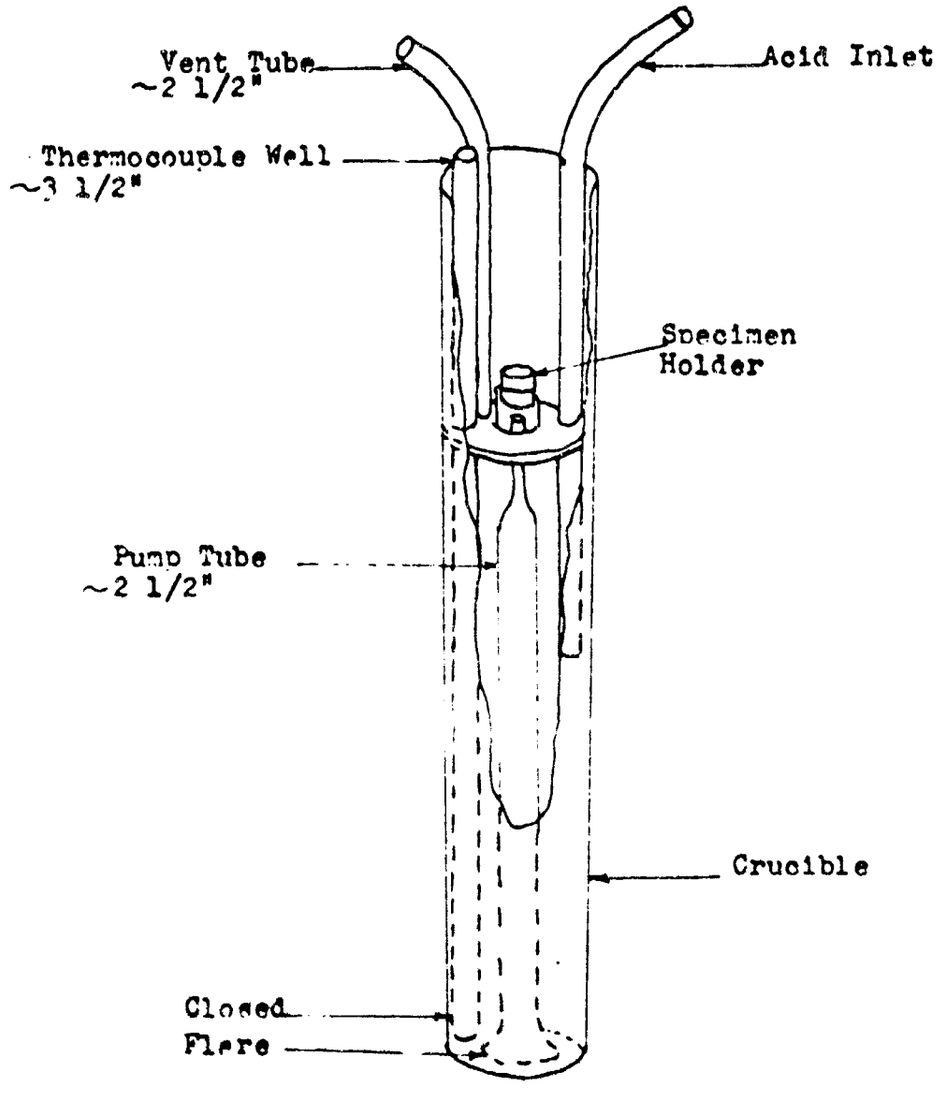

Fig. 4--Jet Thinning Device

c. Results and Discussion

The results obtained are shown in Figs. 5a and 5b, A-L.* Figure 5aA shows a dendritic formation on the GR 755** sample (magnification 10,800). The selected area diffraction pattern is very diffuse and could not be properly photographed. All evidence indicates that this region is a region of aluminum phosphate formation. Dislocations were not observed in this area. Selected area diffraction photographs of the dark and light areas were taken and a low degree of crystallinity found. These photographs did not have enough contrast to be shown in this study.

Figure 5aB is a transmission photograph (6600x) of another area of the same sample. Here an interesting precipitate distribution is noted. The selected area diffraction pattern of the above area is shown in Fig. 5aC. Diffraction patterns similar to his were obtained for all the regions examined. Due to the low order of crystallinity, it is felt that these areas are partially amorphous and are the reaction products of Al_2O_3 and H_3PO_4. This sample was held for 1-1/3 minutes at 450°C in the thinning device.

Any d-spacing calculated with the electron microscope is only accurate to, at best, somewhere in the second decimal place. Therefore the electron microscope could not be used for solid solution or accurate d-spacing measurements.

Another sample taken from the same fired specimen was thinned for 1-1/2 minutes at 450°C. Figure 5aD is a transmission picture at a magnification of 10,200x. A set of fine lines can be seen at the boundary between the thick and thin regions. These are interference figures caused by the change in thickness. No dislocations are seen in this area. Certain dark regions are noted which may be due to impurities, but are probably due to localized non-uniform thinning. Figure 5aE is a selected area diffraction photograph of the white area indicating a high degree of crystallinity. Figure 5aF is a selected area diffraction image of the dark area. Both areas are similar; the darker areas shown in Fig. 5aD are undoubtedly due to thicker areas rather than impurities. Figure 5bG is a diffraction pattern of the whole area. If these diffraction patterns are compared, similarities can be noted.

Figures 5bH-5bJ are transmission pictures of another area of the same sample. These figures are at magnifications of 28,600, 50,000 and 41,600x respectively. The last figure is a dark-field image of the same area shown in bright field (Fig. 5bI). The similarity exhibited in these last two figures means that no dislocations are present in the area under examination. If dislocations were present, they would be seen as fine black lines on a positive print. They are due to the different angle of the Bragg reflection. This Bragg reflection from the dislocation is displaced from the apparatus and therefore appears black. If dark field is now used (the aperture is moved to a position where the diffracted beam

*This work was performed with the help of Dr. S. Weissmann and Dr. H. Yamamoto of the Materials Research Laboratory of the College of Engineering, Rutgers University.

**For coding system of samples, see page 15.

A

B

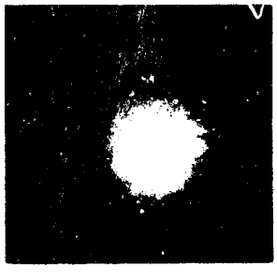

C

D

E

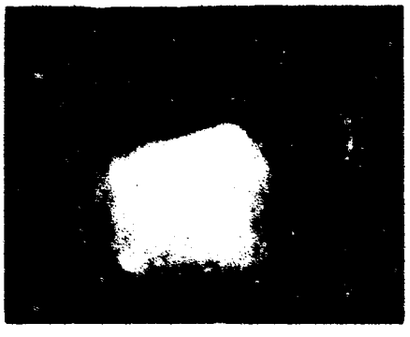

F

Fig. 5a--Photographs of samples examined under the electron microscope.

G

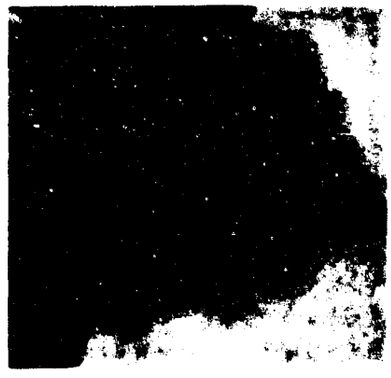

H

I

J

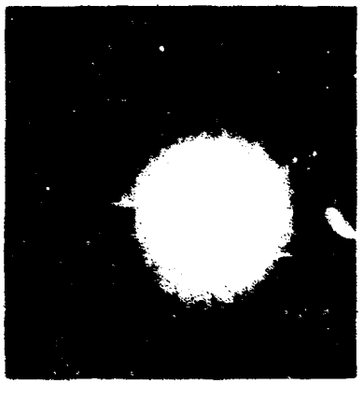

K

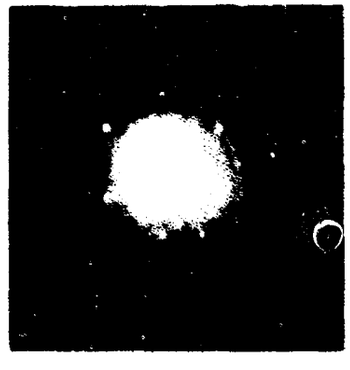

L

Fig. 5b--Photographs of samples examined under the electron microscope.

of the dislocation is transmitted through the aperture), the dislocation will appear white on a positive print. Figures 5bK and 5bL are diffraction pictures of the entire area and the dark area respectively. It can be seen in the first figure that the crystal under observation is hexagonal and the plane being viewed is a basal plane. This crystal must be alumina. In addition, it appears from the diffraction pattern that an alumina crystal, or part of an alumina crystal, is at a different orientation. Figure 5bL is a selected area diffraction pattern of one of the dark areas in the transmission photographs.

The coding system adopted for this work entails a letter for composition, numbers for firing temperature and time, and symbols for firing atmosphere. The specimen CR755H can be identified from the following table.

CR755H

Composition	Temperature	Time	Atmosphere
C = 100% Al_2O_3	5 = 1550°C	1 = 1 hr.	H = hydrogen
R = 99.75% Al_2O_3, 0.25% MgO	6 = 1650°C	3 = 3 hrs.	v = vacuum
CR = 98.0% Al_2O_3, 2.0% MgO	7 = 1700°C	5 = 5 hrs.	He = helium
	75 = 1750°C	7 = 7 hrs.	

Barber and Tighe have shown that as-grown single crystals of alumina oxide, produced by the Verneuil method, have dislocation densities of about $10^2/cm^2$ (Ref. 20). This corresponds to between 1 and 10 dislocations per field of view with the electron microscope. In the case of Linde A, made by calcining aluminum alum, the dislocation density because of temperature, thermal gradients and freedom of expansion, is most probably much less than single crystals--at least in the grain interior. If the dislocation density is assumed to be about $10^3/cm^2$, then 0.1 dislocations would be seen in the entire field of view. It seems reasonable to conclude that few, if any, dislocations would be visible under the electron microscope.

From the very limited data obtained, it is tentatively concluded that sintered alumina of this type has few, if any, dislocations within the grain. If this is true, dislocation may not play a significant role in the sintering process of aluminum oxide. This is substantiated by the sintering literature, which shows that plastic flow is not the mechanism of sintering of alumina. More work is needed before a definite conclusion can be made. Because the magnification is much lower and dislocations, if present, could be more readily seen, optical microscopy studies would have to be included.

4. Role of Magnesia

a. X-Ray Techniques

i. General

Normal x-ray diffraction was used in conjunction with the optical microscope to determine second phase formation. In order to observe the second phase by x-ray diffraction, more than a few percent of this phase must be present. This method was used only to substantiate the results obtained from the study made with the microscope. However, the x-ray back-reflection camera technique was

used to attempt to determine if there was any solid solution of magnesia in alumina. This method yields the most precise values of d-spacings (Ref. 28). At higher Bragg angles, the accuracy of the d-spacings determined by this technique increases. If a change is found when a comparison is made between the pure alumina and alumina plus magnesia compositions, it can be attributed to the solid solution of magnesia in alumina. No noted change in d-spacing can be attributed to one of the following:

1) There is no solid solution of magnesia in alumina.
2) The amount of magnesia going into solid solution is small and the d-spacing associated with it cannot be detected.
3) The magnesia going into solid solution is more highly concentrated near the grain boundaries. Therefore, its solubility towards the middle of the alumina grain decreases to a very low level. Since this technique measures the average value through the grains, the d-spacing change may be too small to be distinguished.
4) Magnesia may go into solid solution interstitially rather than substitutionally.

ii. Procedure

Samples of the 100% Al_2O_3, and the 1/4% MgO-99.75% Al_2O_3 compositions fired for 7 hours at 1550 and 1750°C were ground in an alumina mortar and pestle. These samples were then passed through a 325 mesh screen. Finely divided silicon was added to each sample as an internal standard and the subsequent batch mixed with vaseline. The resultant paste was put on a plastic sheet and placed in the back-reflection camera. In addition to the above samples, a back-reflection x-ray photograph was taken of the Linde A alumina starting material mixed with some of the silicon standard.

The silicon powder used as an internal standard had the following composition:

Si--96.8%	Mn--0.03%
Fe--0.65%	C--0.008%
Ca--0.73%	P--0.008%
Al--0.65%	S--0.005%
Ti--0.10%	

D-spacings and corresponding 2 θ values were calculated from the ASTM tabulated values of the lattice dimensions of silicon. Silicon has the diamond structure with an A_o value of 5.431 Å. The formulae used to calculate d-spacings and 2 θ values are as follows (Ref. 28):

$$d = A_o/(h^2 + k^2 + l^2)^{\frac{1}{2}} \qquad (3)$$

$$n\lambda = 2d \sin\theta \quad \text{(Bragg equation)} \qquad (4)$$

where

d = distance between lattice planes
h, k, l = Miller indices of a particular plane
λ = x-ray wave length (used CuK_{α_1})
θ = Bragg angle
n = order of the reflection

On this basis, the following are the (h, k, l), d and 2 θ values that were used for silicon:

h k l	d	2θ
(444)	.78392	158.6°
(533)	.82828	136.85°
(620)	.85866	127.54°

The choice of the samples investigated was dictated by the probability that magnesia in solid solution with alumina would tend to go into solid solution preferentially at or near the grain boundary. Because of smaller grain size, the samples fired at 1550°C may have more grain boundaries than the samples fired at 1750°C. If the amount of MgO in solid solution remained constant as a function of temperature, the change in d-spacing would be more noticeable. If the limit of solid solution increases with temperature, as is normally the case, then it might be expected that the higher temperature material would show an equal or greater indication of solid solution. The pure alumina composition that was fired at 1550°C was used to compare the d-spacings of the magnesia-containing compositions to the pure alumina composition. To determine if the pure alumina sample was contaminated by the magnesia samples, since they were fired at the same time, the pure starting material was also evaluated.

The films were exposed to x-rays for six hours and then developed. Values of 2 θ were determined of both the unknown and internal silicon standard according to the following formula (Ref. 28):

$$2\theta = 180 - \frac{3L}{4r} \qquad (5)$$

where L = distance in mm between corresponding lines.

The minimum errors possible with this technique should be: 3×10^{-4} Å at 120° (in 2 θ) and 1.8×10^{-4} at 150° (in 2 θ). The experimental error using this technique was found to be ±0.1 mm. In the range of 2 θ's used, this would correspond to an error in d-spacing of $\pm 5 \times 10^{-4}$ Å to $\pm 2 \times 10^{-4}$ Å.

X-ray diffraction photographs using the back-reflection camera were made on the following materials:

1) Linde A powder + Si powder (starting material plus standard)
2) pure alumina composition fired for 7 hours at 1550°C in hydrogen + Si powder
3) 1/4% magnesia-containing composition fired for 7 hours at 1550 and 1750°C in hydrogen + Si powder.

Table I

COMPILATION OF 2 θ VALUES DETERMINED FOR Al_2O_3 AND Al_2O_3 + 0.25% MgO USING THE BACK REFLECTION X-RAY CAMERA

Linde A + Si	C57 + Si	R57 + Si	R757 + Si
153.6 - Si	153.6 - Si	153.6 - Si	153.6 - Si
152.4	152.4	152.4	152.4
151.2	151.1	151.1	151.2
150.3	150.1	150.1	150.2
149.3	149.2	149.2	149.2
146.1	146.1	146.1	146.1
145.2	145.1	145.1	145.2
143.1	143.0	143.0	143.1
142.4	142.3	142.3	142.3
136.9 - Si	136.8 - Si	136.8 - Si	136.8 - Si
136.1	136.1	136.1	136.1
131.6	131.6	131.6	131.7
131.1	131.0	131.1	131.1
130.6	130.5	130.5	130.5
129.9	129.8	129.8	129.8
128.3	128.2	128.2	128.2
127.7 - Si	127.6 - Si	127.7 - Si	127.6 - Si
	124.5	124.5	124.6
	122.5	122.5	122.5
	122.0	122.0	122.0

iii. Results and Discussion

All data is presented in Table I above and the errors have been previously tabulated. The values obtained for the silicon standard are the same, within experimental error, for all four samples. Therefore a direct comparison of the 2θ values for aluminum oxide with and without magnesia present can be made. From the data shown, no indication of solid solution of magnesia in alumina is evident for any sample. The grain size effect on solute solubility (preferential solution at the grain boundaries) is not evident. The possible greater solubility of magnesia in alumina as the temperature was raised is also not seen.

These results indicate that if solid solution of magnesia in alumina is present, the amount is below the limit of detection by this technique. In addition, if a concentration gradient solid solution exists, this method will only measure the average value, which would be less than that found in regions of high magnesia concentration near the grain boundaries. Magnesia could also go into solid solution interstitially and any accompanying change in d-spacing, especi-

ally at these low percentages, would not be measurable. Even the 1/4% MgO-containing composition has a large portion of the magnesia bound in spinel crystals.

Jergensen and Westbrook found by microhardness measurements at 1830°C that magnesia enters the alumina structure in solid solution in and around the grain boundary area. They also attempted, by using an electron microprobe analyzer, to demonstrate that MgO was segregated at the grain boundaries. Their attempts failed. They used the back-reflection camera to determine lattice parameter measurements as a function of grain size and reported variations of $2\text{-}3 \times 10^{-3}$ Å change in d-spacings with an alumina composition containing 0.05 wt. % MgO. Their theory was that magnesia is segregated at the grain boundaries and as grain growth (elimination of grain boundaries) proceeds, most of the excess magnesia must be incorporated into the alumina grains (Ref. 29).

Using the back-reflection camera, these present measurements indicate that no measurable change in d-spacing occurs. This was done as a function of either grain size or firing temperature with the same magnesia-containing composition, or in comparison with the pure alumina samples. It seems highly improbable that a change in d-spacing of $2\text{-}3 \times 10^{-3}$ Å could be detected by an addition of 0.05% of an additive. Since their electron probe analysis, which analyzes very small areas to an accuracy of 50 μm, proved unsuccessful, it seems very unlikely that the back-reflection camera, which measures the average value of an extremely larger volume of material, can be more sensitive. Jergenson also suggests, from the results of microhardness measurements, that MgO already segregated at the grain boundaries enters the Al_2O_3 grain to a large extent. This is in direct disagreement with the proposed mechanism of magnesia's inhibition of exaggerated grain growth by retarding grain boundary velocity. Because in nearly all systems examined in the literature the change in d-spacing by the addition of a solvent in solid solution is $\sim 5 \times 10^{-3}$ Å for a 1% addition, this change in d-spacing seems very excessive. In the case of an addition of 0.05%, the change in d-spacing should be $\sim 2 \times 10^{-4}$ Å. This value is well within the minimum experimental error. If a change in d-spacing of the order of magnitude shown by Jergensen is valid, the change would have been observed. At 150° in 2 θ a variation of $\pm 1 \times 10^{-3}$ Å would cause an angular variation of $\pm 0.5^\circ$ in 2 θ. This value is well beyond the experimental error of $\pm 0.1^\circ$ in 2 θ.

b. Electron Probe Analysis

i. General

The electron probe is a valuable new tool in the study of micro variations in materials. It is extremely useful in diffusion studies, segregation effects, etc. (Refs. 29-33). An electron probe was used to investigate how and where magnesia enters the structure of the sintered alumina sample in the following phases:*

1) solid solution of magnesia in alumina
2) gradient of this solid solution, i. e., from the grain boundary to the grain interior.

---

*This work was done with the help of Corning Glass Works. Special credit is due to J. Zitterman, W. Whitney and M. Charters of Corning Glass Works.

3) compositional variation through the grains of the spinel phase, i. e., the solid solution variation of Mg in the spinel grains.

If magnesia goes into solid solution with alumina, it enters the structure with a probable production of vacancies. If there is a gradient of this solid solution, a vacancy concentration gradient can be produced. It can be seen that this concentration gradient will increase from the interior to the surface of the grain from theoretical considerations (the less dense packing and higher energy of the surface). Since the concentration gradient of vacancies is a driving force for sintering, a comparison of these data with the sintering data should show how and why magnesia effects the densification of alumina. The variation of the above-mentioned effects was studied as a function of both time and temperature.

Electron probe microanalysis is actually a microfluorescent analysis method. Electrons from an electron gun are focussed to nearly a point source (0.3 microns). These accelerated electrons impinge on the sample in a diameter of approximately 0.5 microns, and the sample is made to fluoresce. The x-rays produced by the sample are reflected off a curved sensing crystal. The crystal is placed at the proper angle and has the proper d-spacings to reflect a certain known x-ray wave length characteristic of the cation being examined. The intensity of this reflected beam can be measured as a function of distance through the sample. Due to scattering, the diameter examined is normally about one to three microns rather than .5 microns. Since aluminum and magnesium are at the lower end of the periodic system, it may be difficult to determine small concentrations of magnesia in alumina. Further, the electrons penetrate to between 5 and 6 microns. Thus the effective fluorescence is from a volume approximately 3 microns in diameter and 5 microns deep.

ii. Procedure

In this method, sample preparation is very critical. Polished sections must be made with smooth and regular surfaces or erroneous results may occur in semi-quantitative or quantitative determinations due to valleys and hills within the sample. The method used in preparing these sections was as follows:

1) The sample was molded in amber Bakelite (used because of its low vapor pressure).
2) It was ground and polished, using the Automet machine.
3) The sample was ground for 5 minutes each on 120, 240, 320, 400 and 600 grit silicon carbide paper.
4) It was polished using six, one, and 1/4 micron diamond p[illegible] 2 minutes each.
5) A conductive carbon coating was vacuum-evaporated on the sample.

After the samples were prepared, they were investigated, using the ARL electron probe.

An accelerating voltage of 30 kv was used with the probe. This results in a penetration of 6 microns into the sample. The fluorescent spot size in this light matrix system (Mg, Al, O) is between 2 and 3 microns. If heavier elements were examined, the spot size would be reduced to values between 1 and 2 microns. This fluorescent spot size is the resolution of the electron probe. Mica and an-

lydrous dihydrogen phosphate were used as sensing crystals in the fluorescent analysis of magnesium and aluminum respectively. In one less sensitive set of data, only the mica crystal was used to determine magnesium percentages. In the more accurate set of data, both sensing crystals were used to determine the magnesium concentration. In order to correlate the data properly, the same magnification (444x) was used for all samples in the more accurate set of data. This magnification was also used to locate a representative area of the specimen. In the less sensitive set of data, a 200-scale deflection was equivalent to 100% magnesium. The more accurate set of data used this amplification. In addition, the signal was further amplified so that a 63-scale deflection was equivalent to 4.75% magnesium by weight. A magnesia single crystal was first used as a standard, but no correlation could be obtained with the samples. A spinel single crystal containing 2.5 mole excess aluminum oxide (obtained from R. Arlett of R. C. A. Research Laboratories) was used next, and correlation with the specimens examined was obtained.

The maximum error in composition found using the electron probe was $\pm 3\%$ of any percentage. Because of the difficulty in estimating the deflection on the recording chart, this error was increased to about 10% for scale deflections between 0.5 and 0.1. The limit of detection of magnesium reported by Zitterman and Whitney (Ref. 32) was between 0.0005 wt. % and 0.01 wt. % magnesium. This limit is only applicable to the more sensitive set of data.

The A. R. L. electron probe can analyze two cations at the same time. Four major types of results can be obtained with the electron probe and are discussed below:

1) back-scatter image. This image can be seen visually on an oscilloscope and recorded pictorially. It is caused by the elastic impact of the electron beam with the sample's electrons. The electrons of the beam are accelerated to the sample and back-scattered. The heavier the element, the more intense the back scatter.
2) X-ray fluorescent image. This image can be seen visually on an oscilloscope or recorded pictorially. It is due to the fluorescence of the whole sample area under the bombardment of the accelerating electrons.
3) Line profile. In this method a line indicating the fluorescent analysis of material crossing a line in the field of view yields the relative percentages of the element under investigation. This technique is not as accurate as the point count method.
4) Point count method. In this method, the beam is moved manually from position to position and the intensity of the fluorescing element recorded on a strip chart. Since this method yields the most precise measurements, it was used for quantitative analysis.

Photomicrographs were made of the polished sections used in the probe analysis. Due to the extreme hardness of aluminum oxide, identification marks could not be placed on the examined area of the sample. The photomicrographs taken are of each sample analyzed, but the areas seen are just representative of each sample--not the actual area examined by the electron probe. The following samples were investigated:

1) 2% MgO-containing composition fired in H_2 for 7 hours at 1750°C.
2) 1/4% MgO-containing composition fired in H_2 for 7 hours at 1750°C.

3) 2% MgO-containing composition fired in H_2 for 7 hours at 1550°C.
4) 1/4% MgO-containing composition fired in H_2 for 7 hours at 1550°C.
5) 2% MgO-containing composition fired in H_2 for 1 hour at 1550°C.

iii. Results and Discussion

Figures 6aC-F and 6bC-J are photographs showing the back-scatter and fluorescent images of the 1/4% and 2% magnesia-containing compositions fired at 1550°C and 1750°C respectively and held for 7 hours at these temperatures. Figures 6aA and 6aB are back-scatter and magnesia fluorescent images of the 2% magnesia-containing composition fired for 1 hour at 1550°C. The magnification used is such that each small division shown is equal to 4 microns. Figures 7A and 7B are photographs of the above sample of the 2% magnesia-doped composition fired at 1750°C. The sensitivity for this set of data is much less than the first set. The magnification with this less sensitive data is twice as high as the more sensitive data. The region shown in the less sensitive set is a region high in magnesia as compared to the low level of magnesia concentration in the other set. Table II is the data obtained by the point count method along lines through the x-ray fluorescent pictures shown previously. It is shown here to exhibit this type of data and will be discussed below. Figures 8A-8D are photomicrographs of the etched polished sections of the compositions used in the probe analysis. The areas shown are representative of each sample, but are not the exact area examined as described above.

These photomicrographs were taken using incident phase contrast at 200x magnification. The grain size can be observed by viewing the picture of the stage micrometer where each small division is 10 microns. Good correlation of grain size exists with the fragmentation method of earlier work. The grain size is similar as determined from the photomicrographs and as reported in the Final Report of Contract NOw 64-0040-d. Some regions of porosity are seen in the high-temperature samples and were found to be caused by grain pull-out.

The data presented will be discussed as sets of (1) back scatter, (2) fluorescent and microstructure photographs with the point count data, and (3) the curves of magnesia percentage vs. distance along a selected line in a specimen. Comparisons will be made of time, temperature and compositional effects.

Figures 6aA-F, 6bC-J and 7A-B (back-scatter and x-ray fluorescent images of magnesia), Figs. 9-14 (graphic representation of the point count results), Figs. 8A-E (photomicrographs of the samples) and Table II (point count analysis of the variation of magnesium concentration with distance) are graphs and tables of analytical information of the samples examined by electron probe analysis. After each sample is discussed, comparisons between samples will be made to illustrate the determined relationships and effects. The evaluation of the information obtained from the back-scatter and fluorescent images will be postponed until discussion of the pure alumina composition fired to 1750°C in hydrogen. This sample illustrates the differences between these pictures best.

Figure 6aB is a photograph of back scatter and Mg fluorescence for composition R fired to 1500° C for 1 hour in hydrgen (CR51H), and shows that magnesium is widely distributed through the area. The grain size observed by the fragmentation technique indicates an average grain size of one to two microns. Phase determinations made by optical microscopy and electron probe analysis (Fig. 6aB)

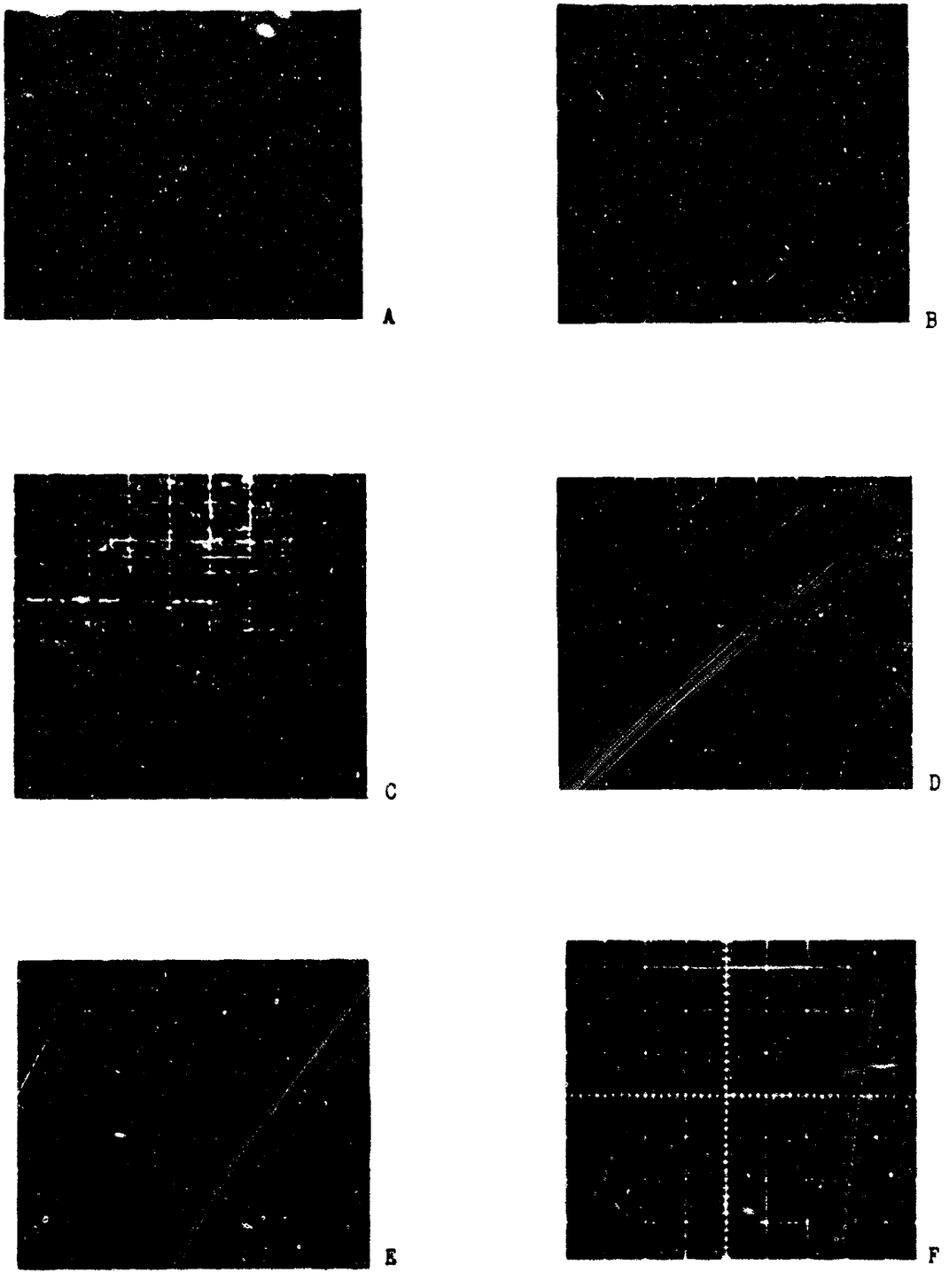

Fig. 6a--Photographs of back scatter and Mg fluorescent images from electron probe analysis. Sensitive data.

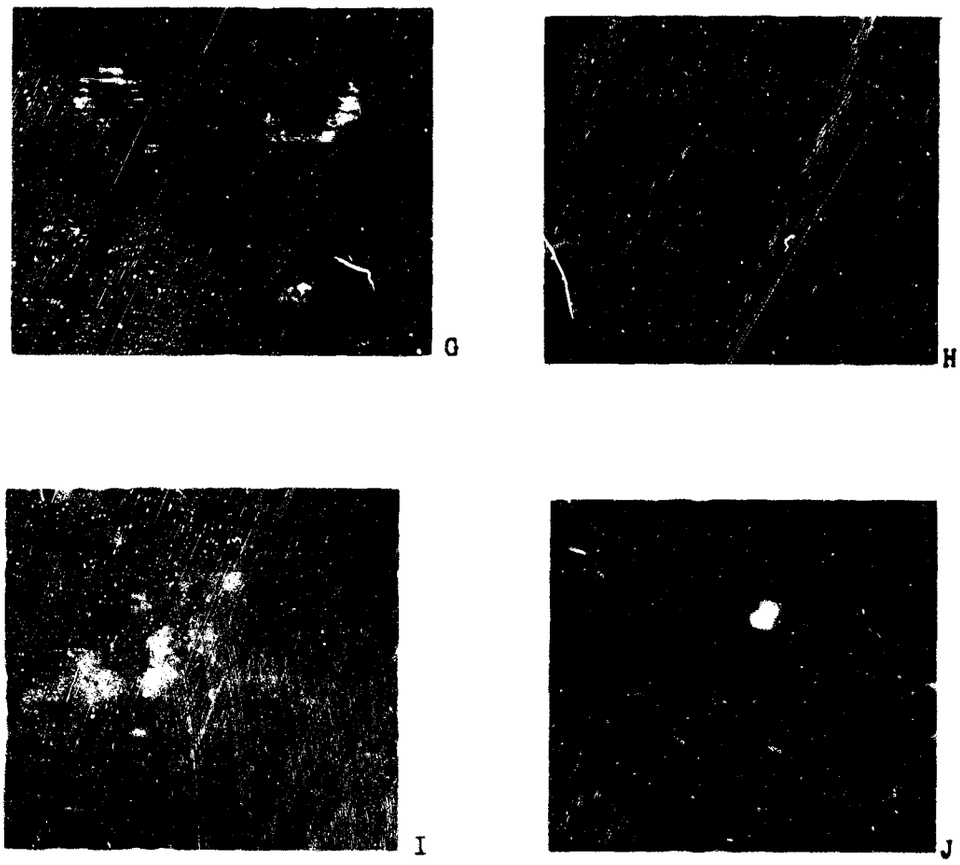

Fig. 6b--Photographs of back scatter and Mg fluorescent images from electron probe analysis. Sensitive data.

A

B

Fig. 7--Photographs of back scatter and fluorescent images from electron probe analysis. Less sensitive data.

Table II

ELECTRON PROBE DATA

(More Sensitive Sets)

Composition CR57H(1) Deflection	CR57H(1) Wt. % Mg	CR57H(2) Deflection	CR57H(2) Wt. % Mg	R57H(3) Deflection	R57H(3) Wt. % Mg
2.8	0.21	3.0	0.23	0.5	0.038
7.5	0.56	5.0	0.38	0.25	0.019
15.5	1.16	2.5	0.19	0.0	0.00
15.0	1.13	2.5	0.19	0.25	0.019
13.0	0.98	2.25	0.17	0.0	0.00
7.2	0.54	12.8	0.96	0.25	0.019
5.0	0.38	5.5	0.41	0.25	0.019
8.0	0.60	3.5	0.26	0.50	0.038
3.2	0.24	2.5	0.19	0.25	0.019
10.5	0.79	7.2	0.54	0.25	0.019
8.2	0.62	8.2	0.62	0.50	0.038
10.25	0.77	3.5	0.26	0.50	0.038
13.2	0.99	2.8	0.21	0.10	0.008
16.8	1.26	3.5	0.26	0.50	0.038
16.0	1.20	5.0	0.38	0.00	0.00
14.8	1.11	0.25	0.019	0.00	0.00
17.8	1.34	0.25	0.019	0.75	0.057
17.25	1.29	0.1	0.008	0.50	0.038
14.0	1.05	0.25	0.019	0.75	0.057
11.0	0.83	0.50	0.038	1.50	0.114
2.8	0.21	0.25	0.019	0.25	0.019
2.25	0.17	0.0	0.00	0.1	0.008
2.0	0.15	0.0	0.00	0.5	0.038
2.0	0.15	0.25	0.019		
0.5	0.038	0.50	0.038		
3.5	0.26	0.25	0.019	Up 0 Left 40	
4.8	0.36			Up 0 Right 6	
4.5	0.34				
Down 10 Left 40		Up 0 Left 40			
Down 10 Right 14		Up 0 Right 10			

(1) 98% Al_2O_3 - 2% MgO 1550° C for 1 hr in H_2
(2) 98% Al_2O_3 - 2% MgO 1550° C for 7 hr in H_2
(3) 99.75% Al_2O_3 - 1/4% MgO 1550° C for 7 hr in H_2

Table II (Cont.)

Composition R757H[1] Deflection	Wt. % Mg	CR757H[2] Deflection	Wt. % Mg	Deflection	Wt. % Mg
12.0	0.95	1.5	0.12	0.5	0.04
12.0	0.95	1.5	0.12	0.5	0.04
1.5	0.12	1.5	0.12	0.0	0.00
1.3	0.10	1.7	0.13	1.5	0.11
1.3	0.10	1.3	0.10	0.25	0.02
1.0	0.08	1.5	0.12	0.5	0.04
2.3	0.18	1.5	0.12	0.5	0.04
0.0	0.00	1.7	0.13	0.75	0.06
2.0	0.16	1.5	0.12	0.0	0.00
9.5	0.74	1.7	0.13	0.75	0.06
25.0	1.98	1.4	0.11	0.5	0.04
22.5	1.78	1.5	0.12	0.5	0.04
14.5	1.15	1.0	0.05	0.75	0.06
1.5	0.12	1.5	0.12	0.75	0.06
1.5	0.12	2.5	0.20	0.5	0.04
1.5	0.12	1.5	0.12	0.5	0.04
0.3	0.02			0.25	0.02
2.3	0.18	Up 40 Left 0		0.25	0.02
4.0	0.12	Up 10 Left 0		1.00	0.08
2.3	0.16			1.00	0.08
4.0	0.12	45.5	3.59	0.00	0.00
2.3	0.18	48.0	3.79	0.5	0.04
1.5	0.12	39.5	3.12	0.3	0.023
2.0	0.16	24.5	1.94	0.75	0.06
1.5	0.12	2.7	0.21	0.5	0.04
14.0	1.11	2.5	0.20	0.5	0.04
12.0	0.95	5.0	0.40	0.5	0.04
12.0	0.95	23.0	1.82	0.5	0.04
2.5	0.20	35.5	2.65	1.0	0.08
1.5	0.12	13.7	1.08	0.5	0.04
0.0	0.00	2.0	0.16	0.75	0.06
1.5	0.12	1.5	0.12	0.5	0.04
2.0	0.16			0.5	0.04
1.5	0.12	Up 30 Left 22		0.5	0.04
4.0	0.32	Up 0 Left 22		0.5	0.04
2.0	0.16			0.25	0.02
1.0	0.08				
2.0	0.16				
15.0	0.12				
1.5	0.12				
1.5	0.12				
2.0	0.16				
1.7	0.12				
Up 10 Left 40					
Up 10 Right 40					

(1) R757H--99.75% Al_2O_3 - 1/4% MgO 1750° C for 7 hr in H_2

(2) CR757H--98% Al_2O_3 - 2% MgO 1750° C for 7 hr in H_2

Table II (Cont.)

ELECTRON PROBE ANALYSIS

(Less Sensitive Data)*

CR757H

Wt. % Mg	Wt. % Al	Wt. % Mg	Wt. % Al	Wt. % Mg	Wt. % Al
0.0	40.8	0.0	43.0--5μ	0.0	44.3
0.0	44.0	0.0	44.8--5μ	0.0	43.8
1.3	41.0	0.0	44.8--5μ	2.5	38.0
1.0	41.38	0.0	45.0	1.4	40.13
3.25	34.8	0.0	44.5	0.0	43.63
2.5	37.5	0.13	43.8--2μ	0.0	44.3
0.75	42.1	0.63	42.5	0.0	45.5
0.0	44.5	2.25	38.3	0.0	44.3
0.0	44.8	2.75	34.5	0.0	44.13
0.0	45.0	1.50	38.5	0.0	43.8
0.0	44.8	0.75	40.63	0.0	43.8
0.0	44.5	0.00	43.13	0.0	43.8
0.0	44.6	0.00	44.0	0.0	43.8
0.0	44.8	0.00	44.3	0.0	44.13
0.0	44.6	0.00	44.3	0.0	43.8
0.0	44.8			0.0	44.0
0.0	44.9	Up 40 Left 20		0.0	44.3
0.25	42.8	Up 0 Left 20		0.0	44.8
Up 10 Left 40 Up 10 Right 40 in 5μ steps				Up 34 Right 30 Up 0 Right 30 in 2μ steps	

*ADP crystal used for Al. Mica crystal used for Mg.

A--R57

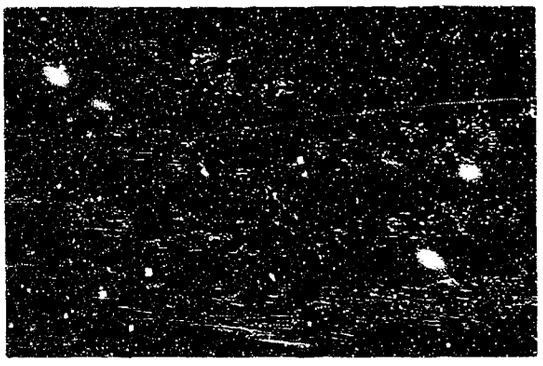

B-CR57

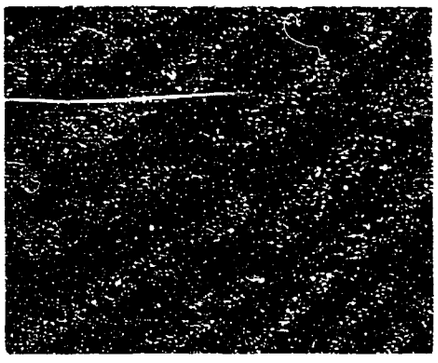

C-CR757

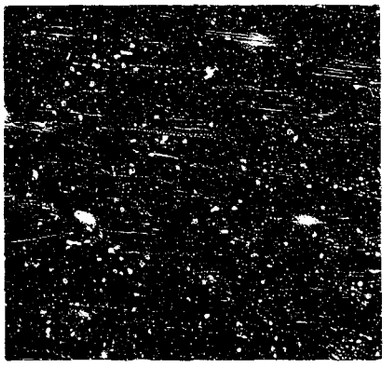

D-R757

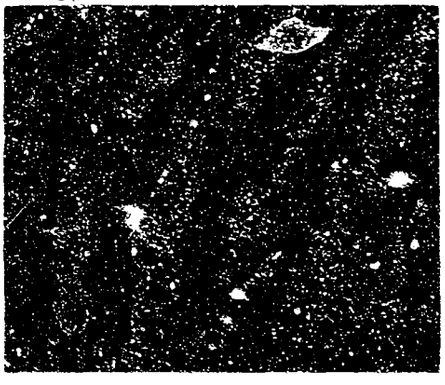

E-Stage micrometer

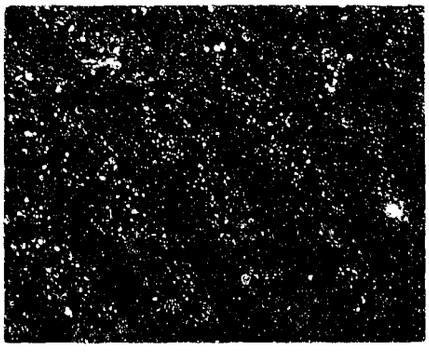

Fig. 8--Photographs of the polished sections used in electron probe analysis (A-D). E, stage micrometer.

Wt. Percent Mg

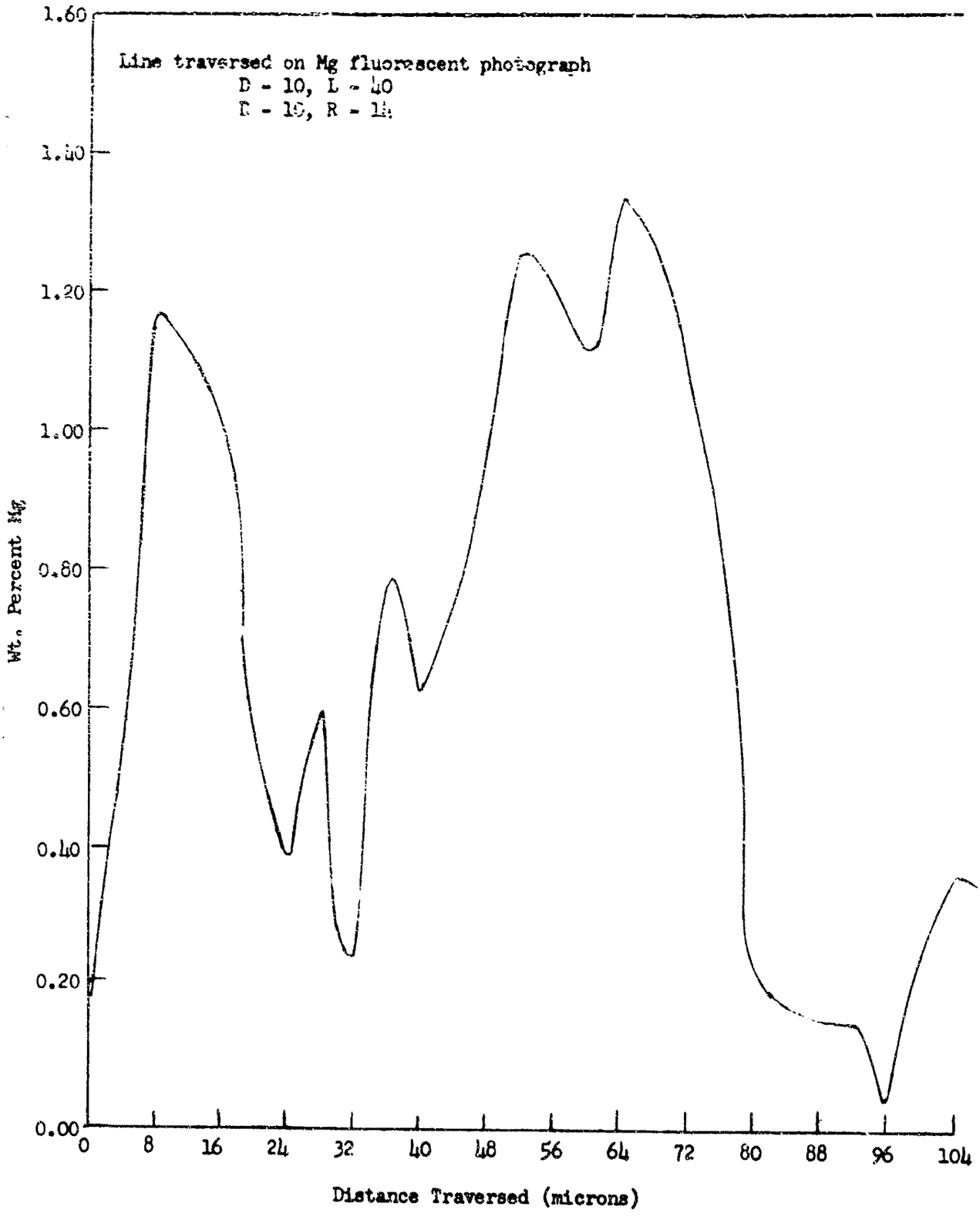

Fig. 9--Point Count for Mg^{++} in Sample CR51 (Sensitive Data)

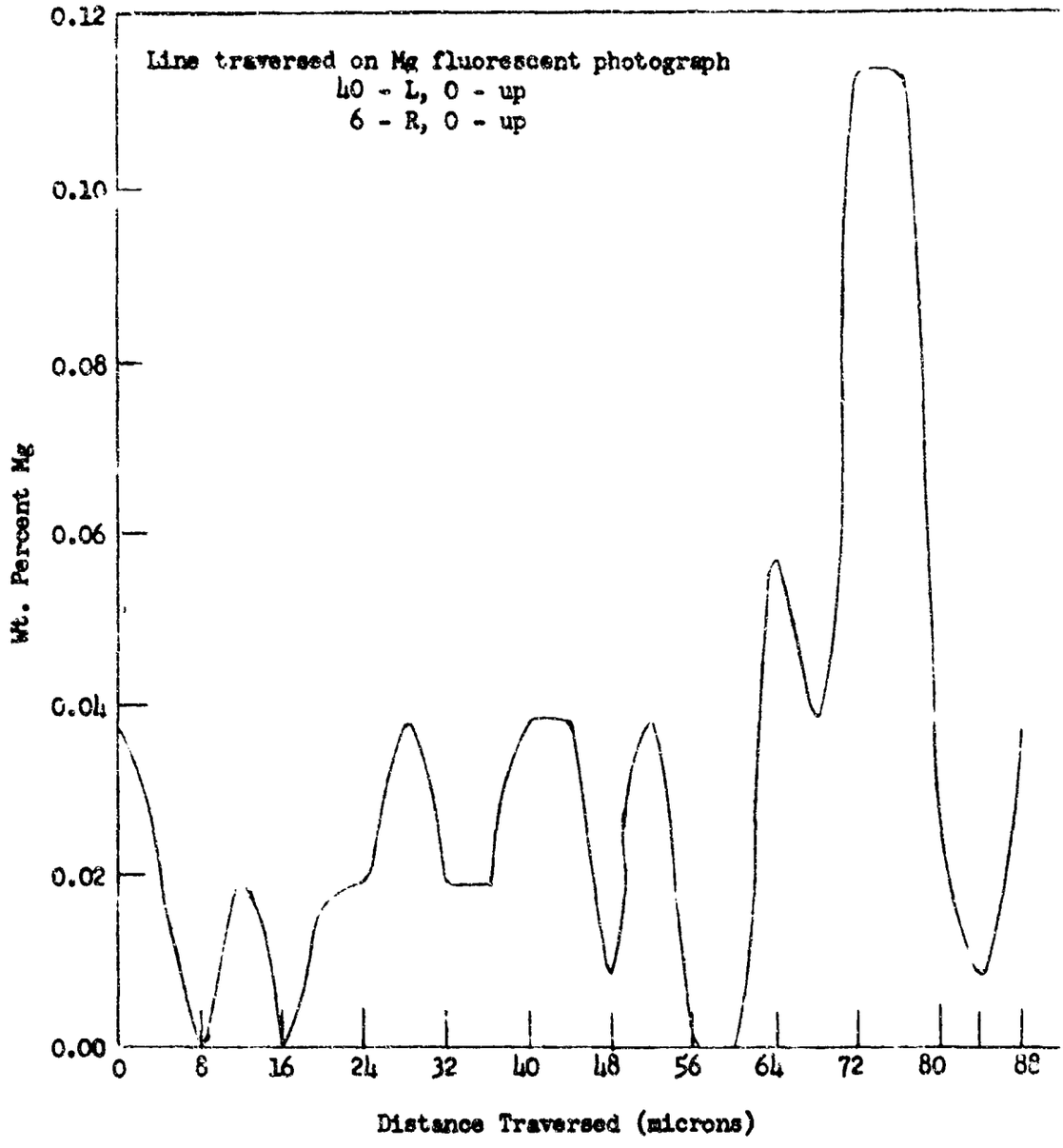

Fig. 10--Point Count for Mg^{++} in Sample R57 (Sensitive Data)

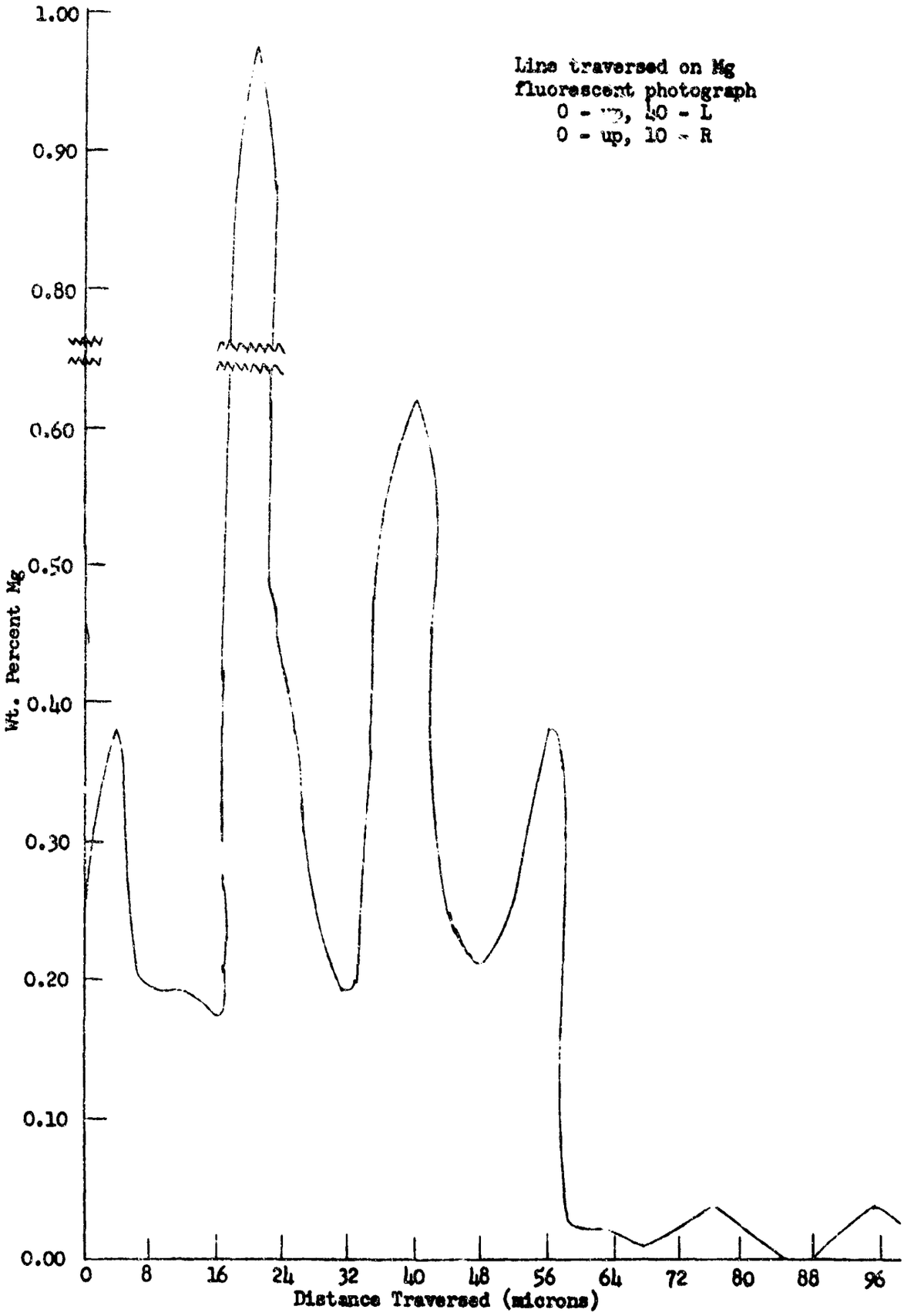

Fig. 11--Point Count for Mg^{++} in Sample CR57 (Sensitive Data)

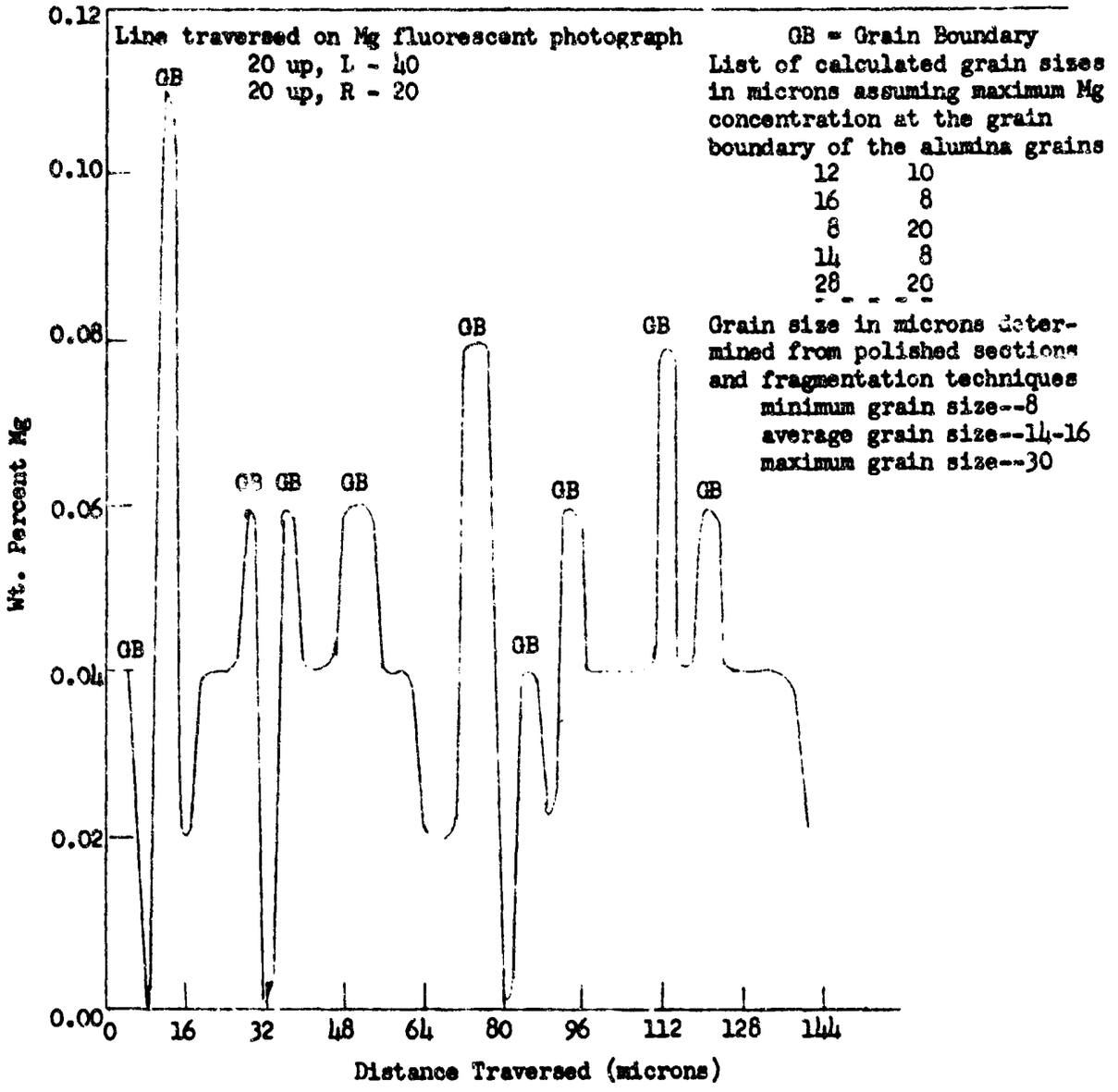

Fig. 12--Point Count for Mg^{++} in Sample CR757 (Sensitive Data)

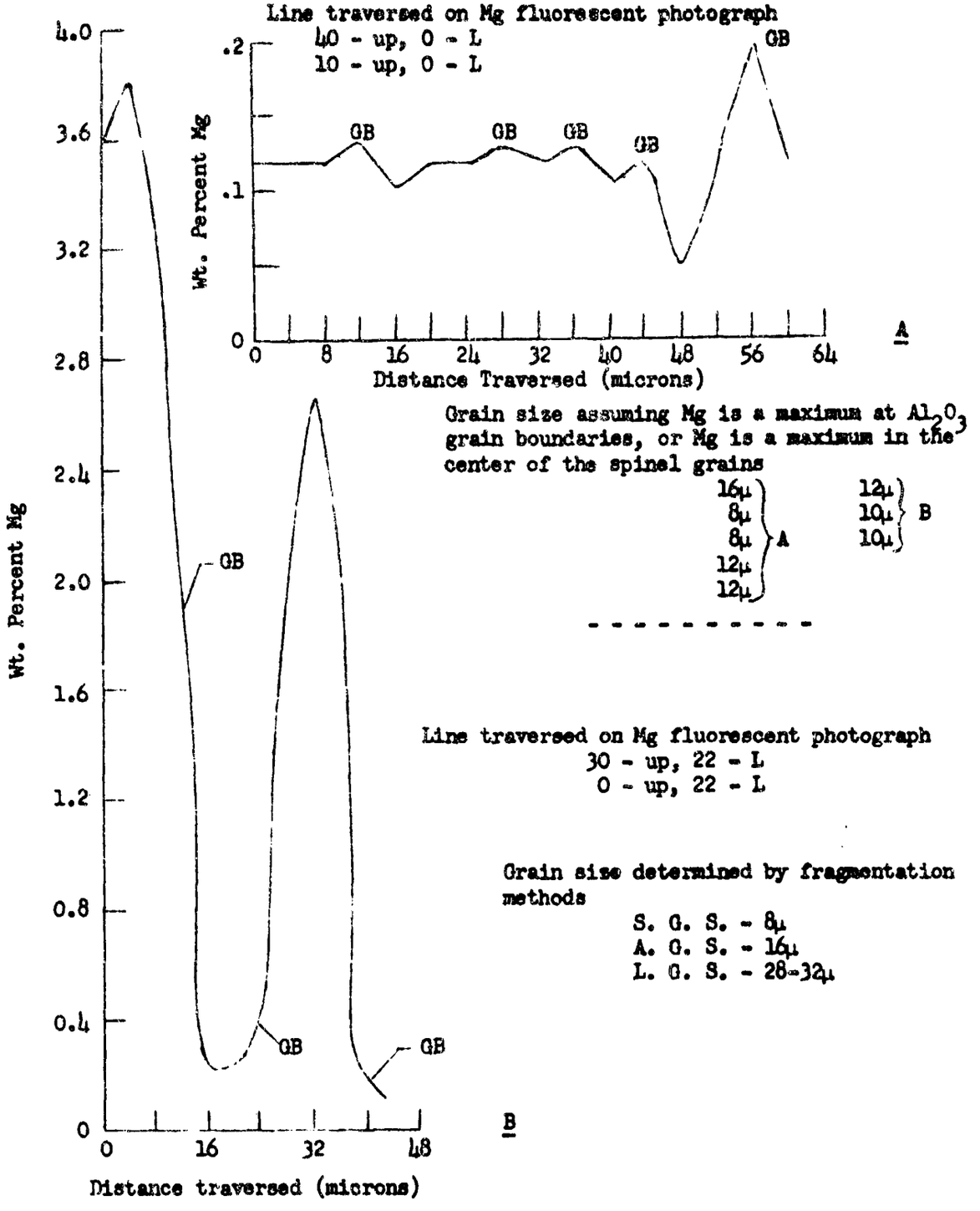

Fig. 13A, B--Point Count for Mg^{++} in Sample R757 (Sensitive Data)

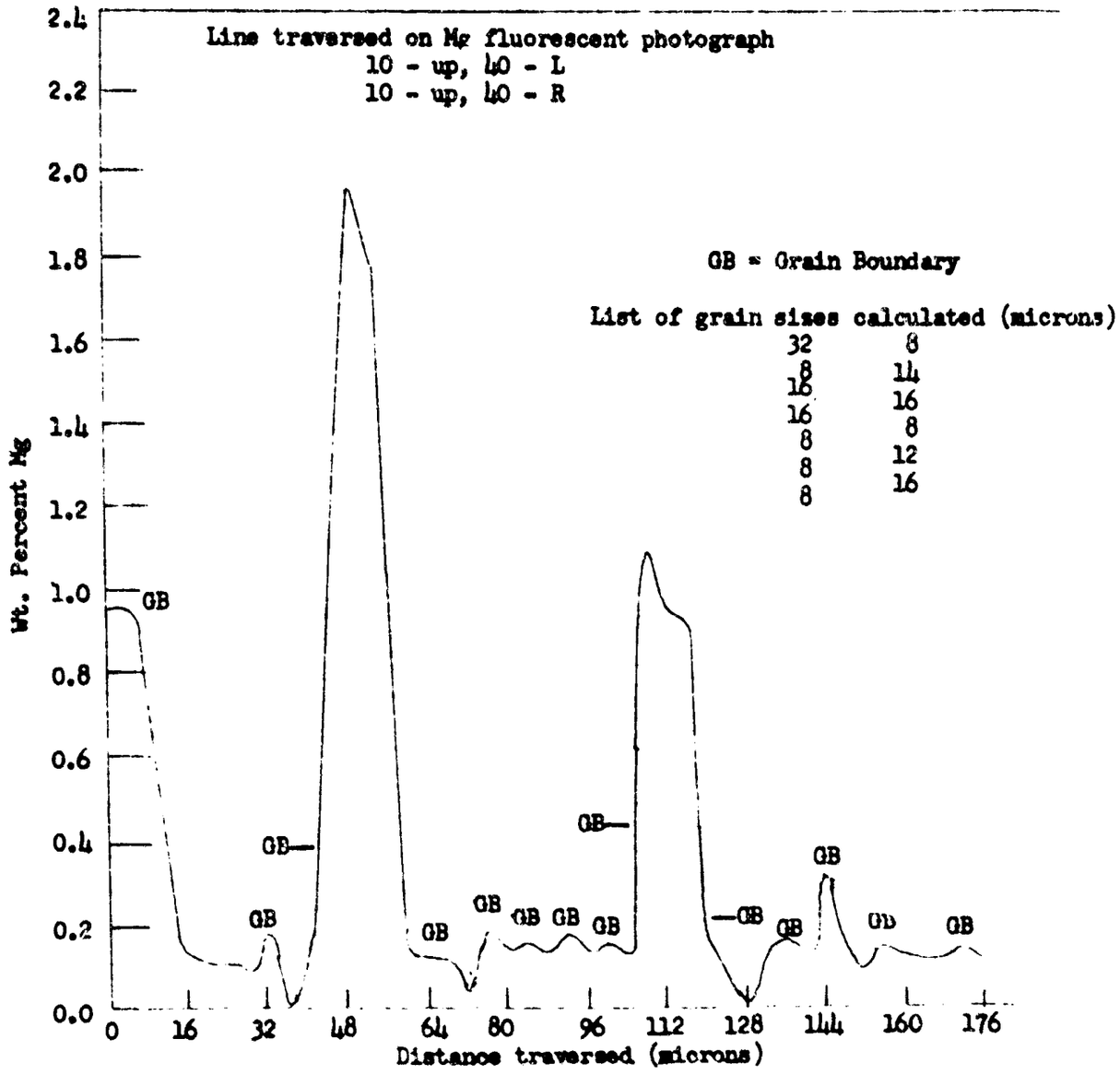

Fig. 13C--Point Count for Mg^{++} in Sample R757 (Sensitive Data)

This is the same sample as used in Fig. 12.

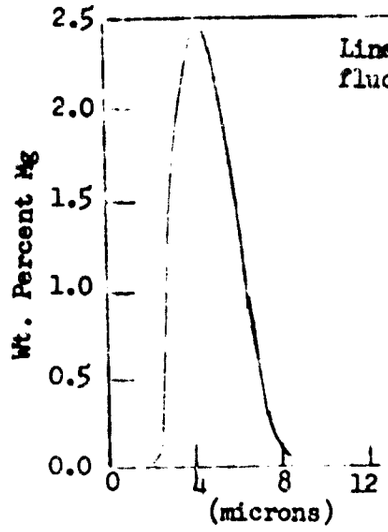

Line traversed on Mg fluorescent photograph
34 - up, 30 - R
24 - up, 30 - R

For all figures: The following grain sizes were calculated assuming a maximum concentration of Mg at the centers of each spinel grain.

6μ 8μ
15μ 6μ
15μ

Line traversed on Mg fluorescent photograph
0 - up, 25 - L
18 - up, 25 - L

Line traversed on Mg fluorescent photograph
10 - up, 40 - L
10 - up, 5 - L

Line traversed on Mg fluorescent photograph
20 - up, 20 - L
6 - up, 20 - L

Wt. Percent Mg

Distance traversed (microns)

Fig. 14--Point Count for Mg^{++} in Sample CR757 (Less Sensitive Data)

substantiate the spinel coating or a fine dispersion of small particles of spinel along the grain boundary found at this temperature. Because of the small grain size and from the data shown graphically in Fig. 9, little can be determined of both spinel or magnesia solid solution. However, it can be noted that magnesia was present at each datum point. This indicated a distribution of magnesia in the sample. Probably because of non-uniform mixing, magnesia is found to be more highly concentrated in some regions than in others. These regions may act as nuclei for the spinel segregation observed at 1750°C.

Figure 6aD is of composition R fired to 1500°C for 7 hours in R57H hydrogen and shows that magnesia is distributed fairly uniformly through the area. The area examined is comparable to the region shown in the central right portion of Fig. 6aB and is probably a little below average in magnesium concentration. From Fig. 8A and the grain size results determined by the fragmentation method, the average grain size is found to be approximately 4 to 5 microns. As seen from the fluorescent image, magnesium is distributed at distances ranging from 3 to 8 microns. This distribution is similar to the determined grain size distribution and agrees with the spinel distribution noted by optical microscopy. Figure 10 is a graphical representation of the magnesium concentration as a function of distance. The low values of magnesium concentration found can be justified by considering that the probe examines volumes between 20 and 50 cubic microns. If the spinel coating is assumed to be 1 to 2 microns thick, as seen from the dot size, and about 1 to 2 microns deep, than only 1/5 to 1/10 of the total volume examined can be spinel. The alumina grain size has increased at this temperature and firing time. If, for example, a solid solution gradient of magnesia from the grain boundary to the grain interior (the interior having a lower percentage) exists, then values of this low order of magnitude should be found. These lower values could also be expected if solid solution does not occur. When comparing the above sample with the previous one, the magnesium concentrations are much less. This is due to either larger grain sizes or less highly localized concentrations in the regions examined. Because of smaller grain size of the CR51H sample, many regions of spinel could be found for each point examined (2 to 3 microns). Therefore, if similar depositions of spinel at the grain boundary are assumed for the CR51H sample, this sample can be expected to yield higher magnesium percentages. Although the point count method is not continuous, about 3 out of every 4 microns are examined. Some regions of solid solution of magnesia in alumina are indicated in this and the next sample, but the evidence is inconclusive. It is of extreme importance to note that the range of magnesium concentration found was between 0.00 and 0.10% and that many areas indicating spinel are seen in this fluorescent analysis. This information is needed to determine whether solid solution is present at higher temperatures.

Figure 6aF for composition CR57H is the magnesium fluorescent picture of the area under examination. The contrast of this print is not particularly good and following the magnesium concentration in this print is not very informative. Fig. 8B is a photomicrograph showing the grain size of this sample. The average determined grain size is about 4 microns with larger grains about 8 microns. Figure 11 is a graphical representation of magnesium concentration vs. distance for this sample. It is noted that regions of 0.00% Mg were found in this and the R57H sample. In order to obtain this result, the probe was most probably positioned at the center of a larger alumina grain. From the above effect, some indication of a solid solution and solid solution gradient of magnesia in alumina was obtained in this and the R57H sample. Because of the comparatively small

grain size, these solid solution effects cannot be conclusively proven from the probe analysis. From (1) the above results, (2) the sintering results which show an enhanced sintering rate with magnesia additions at all temperatures investigated, and (3) the results obtained with the high-temperature samples using the electron probe, a solid solution and/or a solid solution gradient can be inferred for both the R and CR (1/4% and 2% MgO) compositions at 1550°C.

The magnesium fluorescent photograph (Fig. 6bH) for this sample CR757H is very informative. As seen from this figure, no indication of magnesium is noted in the entire field of view. Many regions similar to this were found in this sample and the R757H sample. This absence of magnesium is not due to poor printing of the photograph, for the same result was seen in the cathode ray oscilloscope. It is important to note that these photographs are not as sensitive as the point count or quantitative mode analysis. A graphical representation of the magnesia concentration along a line through the black picture is shown in Fig. 12. Figure 8C is a photograph showing the grain size of this sample.

A very low level of magnesium concentration is seen from the graph. This low concentration is indicative of the solid solution of magnesia in alumina. Since the area within individual grains may be examined without encountering a grain boundary, the grain size (small grain size 8-10 μ, average grain size 15 μ, larger grain size 20-30 μ), as seen in Figs. 8C and 8E, may be too large to propose that widely distributed small spinel particles at the grain boundary would yield this low level of concentration. Individual particles or small regions of spinel at the grain boundaries were observed in the R57H sample. A similar effect was noted for all the low temperature samples investigated, except that the concentrations in this sample and the R57H are extremely similar. In the case of the CR757H sample, the magnesium fluorescent image is absent. From thermodynamic considerations and because of the higher energies needed, it is not very likely that magnesium is distributed as very small spinel particles through the alumina grain. If this low concentration was caused by a dispersion of small spinel particles through the alumina grain, then the magnesium fluorescent image would be speckled with small dots which indicate highly localized regions of magnesium, as noted in the R57H and other low-temperature samples. Since the magnesium fluorescent image was black and dots indicating spinel are not present, and since the concentrations of magnesium determined with this sample and the R57H sample (whose fluorescent image showed these dots) are nearly identical, a solid solution of magnesia in alumina may exist. Therefore it is concluded that a solid solution of magnesia in alumina probably occurs at 1750°C. A further example of this effect will be shown with the R757H sample.

Another important deduction can be made if the average grain size and grain size distribution for the sample and the region examined are assumed the same. If it is also assumed that the maximum magnesia concentration in the solid solution of magnesia in alumina occurs at the grain boundary, then a determination of grain size via the graphical representation of the point count method can be made and compared to actual grain size found by the fragmentation and polished section method from earlier work and shown in Fig. 8C. This comparison is shown by Fig. 12. It is seen that good agreement is obtained when comparing the calculated grain size (Fig. 12) and the measured grain size. It is therefore felt that a solid solution gradient of magnesia in alumina exists in this sample. Since an enhanced sintering rate relative to pure alumina was observed at 1550°C

and 1750°C, and since this solid solution and gradient of solid solution can cause an increased sintering rate by producing a vacancy concentration and concentration gradient, a solid solution and solid solution gradient can be inferred for the 1550°C magnesia-containing compositions. In addition, electron probe analysis showed some slight indication of a solid solution at 1550°C. Using microhardness measurements, Jorgensen and Westbrook reported a solid solution of magnesia in alumina at the grain boundary at 1830°C (Ref. 29). From thermodynamic and kinetic viewpoints, it seems probable that if a solid solution of magnesia in alumina exists, a higher concentration of magnesia should be found in the vicinity of the grain boundary.

Although the area seen in this set of figures is one of the very low magnesium concentrations, other areas on this sample noted in the less sensitive set of data contain much higher concentrations.

The comparison between the back-scatter and magnesium fluorescent images has been postponed until discussion of this sample A757H (Figs. 6bI and 6bJ). If the dark regions on the back-scatter image are noted and compared to the magnesium fluorescent image, it can be seen that nearly every dark area on the back-scatter image corresponds to a region of high magnesia concentration on the fluorescent image. The grain size for this sample is in agreement with earlier petrographic results. A picture of the grain size found with the polished section method is shown in Fig. 8D. Figures 13aA and 13aB and 13bC are graphical plots of the magnesium content vs. distance for the several regions examined.

The first significant point of note is that a segregation of magnesium into regions of high concentration occurs with this sample. From the photographs, these magnesium regions are fairly large and correspond to spinel grains. The same type spinel grains were found from optical microscopy studies and were mentioned previously. From the above discussion, it can be shown that magnesia tends to segregate into localized regions forming spinel grains of comparable size to the best alumina grains at 1750°C. Spinel may segregate into localized regions by one or both of the following mechanisms:

1) From a thermodynamic viewpoint, regions of higher local spinel concentrations at 1550°C can coalesce at 1750°C into large spinel grains to reduce their interfacial and surface energy.

2) An incompatibility between alumina and spinel may exist because of a possible high interfacial energy between them.

The spinel formed is probably a high alumina-spinel solid solution (i. e., 3.5 mole excess Al_2O_3). The excess alumina spinel has a magnesium concentration of 4.8 %. Since a comparatively large volume is examined (50 cubic microns) and these volumes probably not only contain spinel but also alumina, the composition of the spinel determined would tend to have lower magnesium concentrations than these calculated. The effect is due to the incorporation of parts of alumina grains. It is assumed that spinel is present if the concentration of magnesium is somewhere above 0.5 wt. % Mg over a significant range. If the magnesium percentages fall below 0.2 wt. % Mg over a significant range, solid solution of magnesia in alumina is thought to occur.

In Fig. 13a it can be seen that there are two spinel grains (area on right).

A similar effect is seen in Fig. 6bJ. If it is assumed that the center of a spinel grain corresponds to the maximum percentage of magnesium, then a solid solution gradient of magnesium in spinel is seen. The phase diagram for the alumina-magnesia system indicates an increase in alumina content in spinel solid solution as temperature increases (Ref. 33). In addition, true equilibrium is probably not reached with the sintered sample. For both of the above reasons, a "core" effect seems reasonable. Since this "core" effect occurs, spinel may have sufficient time to rearrange itself and subsequently form cube edges. This effect may explain the occasional formation of cubes of spinel found in the sample as noted by optical microscopy. When the grain sizes of the spinel crystals are computed from the graph (Figs. 13aA-B and 13bC), they are found to be similar to those observed experimentally.

As seen from the fluorescent images of the R+CR757H samples, the regions which are either hazy or black may be indicative of solid solution of MgO in Al_2O_3. The point count measurements in these regions show Mg concentrations of 0.2% and less. The grain sizes were 5-10 times greater than those of the low temperature samples. Therefore, the probability of encountering grain boundaries is much less for each datum point. If (1) the Mg concentration found was due to small concentrated inclusions in grains or along grain boundaries, and if (2) the inclusions were of comparable size (1 μ) to the R57H sample which had similar concentrations, then dots or lines indicating localized Mg regions should be detected. If 80-90% of 0.2% Mg or less regions are examined, a solid solution of MgO in Al_2O_3 can be established. In the case of the remaining 10-20%, the Mg concentration drops abruptly to 0. This is diametrically opposed to the first data set indicating that diffusion, and therefore solid solution, is nearly nonexistent. Boundary absorption can be theorized in explanation, but it would be in disagreement with the results obtained 80-90% of the time. If boundary absorption occurs, it would have to extend for 0.1 μ or less into the Al_2O_3 grain. If greater absorption occurred, then spots or lines would be seen on the fluorescent photographs. This low rate of Mg diffusion in Al_2O_3 is not in keeping with the literature. Further examination of these samples is needed. If this last effect is not observed or a gradual transition to 0% Mg is found, then solid solution would be established. A solid solution of MgO in Al_2O_3 is tentatively concluded, since (a) most regions indicate solid solution, (b) sintering is enhanced with MgO, (c) appreciable diffusion rates of MgO in Al_2O_3 have been reported, and (d) inhomogeneities such as those shown are probably not representative of the sample.

Figures 13aA-B and 13bC show that the size of the alumina grains calculated on the assumption that excess magnesia in solid solution with alumina tends to segregate at the grain boundaries is in agreement with the experimentally determined grain size (Fig. 8D and earlier petrographic results). It is felt that this sample, as well as the CR757H sample, shows a solid solution gradient of magnesia in alumina.

Another region of the CR757H sample examined previously is shown in Figs. 7A, 7B and 14. Only spinel grains can be examined with this less sensitive data. It explains why the 2% magnesia-containing composition seemed to have less magnesia present than the 1/4% magnesia-containing composition. The sample is also presented to give further evidence that a solid solution gradient of magnesia exists in spinel.

D. Summary of Results and Discussion of the Entire Program (B and C above)

1. General

The sintering characteristics of alumina were determined as a function of temperature, time, firing atmosphere and concentration of magnesia additions. The lowest temperature at which pure alumina compositions can attain less than 1% total pore volume is 1550°C (2822°F). This is realized by a 2% addition of magnesia and firing in a vacuum with a soak period of 3 hours; this quality is attained with a 1/4% magnesia addition only after a 7-hour soaking period. A hydrogen firing atmosphere necessitates a firing temperature of 1650°C (3000°F) plus a 1-hour soak with both the 1/4 and 2% magnesia additions; a 4-hour soaking period is necessary if a helium atmosphere is used. The total pore volume of the pure alumina compositions, that is, no magnesia additions, never becomes lower than 1.9% even at the highest firing temperature and longest soaking period. To approach theoretical density or a total porosity less than 0.1%, it is necessary to fire to 1750°C in either vacuum or hydrogen. The 1/4% magnesia composition reaches this with a 1-hour soak while the 2% takes 3 hours.

An intensive study of the structure of this composition and the mechanism that produced it was undertaken. An investigation of the phases formed and their distribution was made, using microscopic and x-ray diffraction techniques. By using the back-reflection x-ray camera an attempt was made to determine if magnesia goes into solid solution with alumina. An investigation of the magnesia distribution in the sintered samples was made, using electron probe analysis. These two methods were used in an attempt to understand the role of magnesia additions in the sintering of alumina. Transmission electron microscopy was used in an attempt to determine the quenched defect structure associated with sintering. Determinations of the activation energy associated with the sintering process were attempted using electrical measurements. Activation energies could not be determined by either method. This was probably due to the complex and numerous effects occurring simultaneously.

The inability to determine activation energies may also be due to a dependence of the diffusion coefficient on the vacancy concentration. If one assumes that this concentration is controlled by entropy considerations, the vacancy concentration will vary exponentially with temperature. If it is assumed that the vacancy concentration is controlled by magnesia solid solution etc., and because the degree of solid solution will have a temperature dependency, this concentration will also vary with temperature. In either situation, a plot of the logarithm of the diffusion coefficient vs. the reciprocal of the absolute temperature would not be expected to yield a straight line.

2. Effects of Atmospheres

The sintering rate was found to be independent of firing atmosphere at high temperatures with either vacuum or hydrogen. This indicates that in the final stages of sintering the rate of diffusion of hydrogen was not a rate-controlling step and that hydrogen diffuses probably as H° or H^{+}. Since helium-fired samples at lower temperatures yielded results similar to hydrogen, and since helium is not likely to react with alumina and produce stoichiometric defects, there is no indication that hydrogen enhances the sintering rate by producing defects at low

temperatures. Vacuum-fired samples had the highest sintering rate at 1550°C. Helium-fired samples showed a higher initial sintering rate at 1550°C than hydrogen. These results can be explained by comparing the diffusivities of the gases and the lack of gas in the case of vacuum. Since hydrogen is larger than helium, the diffusivity of hydrogen (H_2, in which form it probably diffuses when open pores are present) is less than helium. The results indicate that at this stage of sintering the over-all rate is partially controlled by gas diffusion. The enhanced sintering rate of helium over hydrogen at 1550°C was found to decrease with time as a function of decreased open porosity. Since helium does not diffuse appreciably through impervious alumina, this relationship is reasonable. At higher temperatures, over-firing, both as a function of time and temperature, was noted in helium for all compositions. This over-firing is due to the inability of helium to diffuse through the structure when open porosity is absent. As the temperature increased, the partial pressure of helium (non-diffusible gas) increased; at the same time the surface energy decreased slowly. Therefore the increased pressure within the pore became sufficient to overcome the surface energy driving force and the body over-fired. The time dependence for this expansion was probably due to a delayed elastic effect, plastic flow or Nebarro-Herring creep. Samples fired in vacuum and hydrogen did not over-fire under the same conditions. Theoretical density was approached by all magnesia-containing compositions in hydrogen and vacuum.

The microstructure results indicate that normal grain growth is not a function of firing atmosphere. Since the vapor-solid surface energy is only very slightly affected by atmosphere, the above result seems quite reasonable. Exaggerated grain growth was found to occur at a lower temperature in helium than either hydrogen or vacuum for the pure alumina composition. A valid explanation was not formed for this phenomenon. Exaggerated grain growth was noted in the 1/4%, but not for the 2%, magnesia-containing composition at 1750°C in helium. This was probably due to the greater degree of inhibition of both normal and exaggerated grain growth found in the 2% magnesia-containing composition.

3. Effects of Magnesia Additions

Under all conditions, the pure alumina composition was found to have a lower sintering rate than the magnesia-containing compositions. This difference in sintering rate is due not only to magnesia's inhibition of exaggerated grain growth or its postulated retardation of normal grain growth (Ref. 34), but also to the enhanced rate due to solid solution or adsorption. At 1550°C, one of the temperatures where this difference in rate was found, no noticeable amount of exaggerated grain growth occurred with any composition fired in vacuum or hydrogen. The grain size of all compositions was similar. The differences in sintering rate between the pure alumina and the magnesia-containing compositions can be attributed to the following:

1) At higher temperatures magnesia inhibits exaggerated grain growth, thereby allowing the compositions containing magnesia to reach theoretical density.
2) Magnesia may form a spinel coating or large numbers of fine spinel particles around the alumina grain and change the surface energy configuration in a way which may aid or hinder sintering.

3) Limited amounts (less than 0.25%) of magnesia may go into solid solution with alumina and also form a solid solution gradient from the grain boundary to the grain interior. Because of stoichiometric considerations vacancies may form and increase the diffusion coefficient. If a solid solution gradient is formed, a vacancy concentration gradient may be built into the system in the proper direction to enhance sintering. If both these effects occur, the sintering rate will increase, since the sintering rate equals the diffusion coefficient multiplied by the vacancy concentration gradient.

The sintering rates for all magnesia compositions are quite similar. Therefore, the sintering rate over this compositional range was independent of the magnesia content but dependent on some critical minimum amount. Bruch (Ref. 35) indicates that similar sintering rates were obtained for both 0.25% and 0.10% magnesia-containing compositions. As seen from the results, all magnesia-containing compositions were beyond the solid solution solubility range of magnesia in alumina. Thus, if solid solution of magnesia in alumina was the major contribution to the enhanced sintering rate, all compositions containing magnesia should have similar rates. If spinel was the contributing factor to the increased rate (excluding case no. 2 mentioned above), it would be compositionally sensitive, but the results did not indicate this.

Because of the absence of magnesia in this pure alumina composition, exaggerated grain growth was found to occur in all three atmospheres. Magnesia can act in the following ways to inhibit exaggerated grain growth:

1) It can change the vapor-solid surface energy, and thereby affect grain growth.
2) By solid solution formation and/or formation of a solid solution gradient, it can increase the sintering rate relative to the rate of grain growth and in this manner by-pass the critical porosity region at a lower temperature. Exaggerated grain growth is then avoided.
3) It can be adsorbed at the surface either as a second phase or a solid solution with a higher concentration of magnesia. In this way, it can act to reduce the maximum grain boundary velocity which would be reached when the pore phase is eliminated in the local region surrounding the grain boundary. In order for the grain boundary to move, the additional magnesia must be carried along with it. Therefore, the grain boundary velocity is lowered.

It is felt that mechanisms two and three are the most probable mechanisms.

The rate of normal grain growth was found to be similar for all magnesia-containing compositions except at 1750°C. Due to greater magnesia concentration at this temperature and long firing times, the 2% MgO-containing composition had a smaller grain size.

Work by Jergensen and Westbrook (Refs. 29, 34) indicated the segregation of magnesia in solid solution with alumina at the grain boundaries at 1830°C. They postulated that at low temperatures during the initial stage of sintering, magnesia in solid solution with alumina near the grain boundaries retards sintering by reducing the diffusion coefficient. They stated that during the intermediate and final sintering stages the sintering rate is enhanced by the incorporation

of magnesia. These authors postulated that retardation of normal grain growth was the mechanism that produced this enhanced rate. This mechanism reduces the distance between the pore and the grain boundary. The retardation of normal grain growth results in an increased vacancy concentration gradient.

It is felt that evidence is insufficient for their conclusions to be valid. They made microhardness measurements at 1830°C that indicated magnesia solid solution at the grain boundary, and unsuccessfully attempted to determine this solid solution by electron probe analysis. However, they found solid solution when using the back-reflection x-ray camera. Jergensen does not consider a temperature dependence for the solid solution of magnesia in alumina when a solid solution is assumed at 1300°C from data obtained at 1830°C. Disagreement of the results and the mechanisms found by Jergensen were previously discussed. Since additional information is necessary for a more detailed investigation of the role of magnesia in the sintering of alumina, the following techniques were utilized:

1) optical microscopy
2) x-ray diffraction
3) back-reflection x-ray camera
4) electron probe analysis.

An attempt was made to determine the activation energy for vacancy movement and relate this to composition and atmosphere. The results obtained indicated that this determination was not feasible.

It is known that defect structure is an important variable whose effects must be understood. Electron transmission microscopy indicated the difficulty in removing the phosphate precipitate formed during thinning from the thin sections. In all the alumina areas examined, evidence of dislocations was not observed. Tighe and Barber have shown that the dislocation density in as-grown single crystals of aluminum oxide made by the Verneuil method is about 10^5 dislocations/cm^2 (Ref. 20). This would correspond to about one to ten dislocations in the entire field of view of the electron microscope. With Linde A the number of dislocations introduced by fabrication and those present initially would probably be much less than in single crystals. Therefore, the dislocation density in the sintered samples should be appreciably less than 10^5 and may be undetectable if examined under the electron microscope. An exhaustive study of very large numbers of grains was carried out; however, dislocations were not observed. Dislocations may be present at grain boundaries in measurable concentrations, but they were not detected. As far as the limited data could be used, the interior of the grain was found to be dislocation-free. Under the conditions investigated, dislocations appear to be of minor importance in the sintering of aluminum oxide. This would tend to support the generally accepted opinion that sintering of aluminum oxide is diffusion-controlled. If the above is conclusively proven, internal dislocations may not act as either vacancy sources or sinks.

Optical microscopy was used to determine the spinel distribution in the sintered samples. The distribution of magnesia was found not to be a function of composition. At 1550°C spinel was found as either a coating or a large dispersion of small particles at the alumina grain boundary. At 1750°C spinel was found in irregular or cubic-shaped grains at the intersection of two or more alumina grains. The latter was observed by the authors and W. C. Allen (Ref. 39).

These results indicate that the solid solution limit of magnesia in alumina at these temperatures is below 0.25% MgO. The ability of spinel to form its own crystal habit may be attributed to the large solid solution variation of Al_2O_3 in $MgO \cdot Al_2O_3$. If this is correct, a solid solution gradient of magnesia in spinel could be formed. Although this gradient was shown, it does not validate the above mechanism. Since a solid solution gradient could also be formed by the non-equilibrium build-up of variable compositioned spinel layers, the above mechanism cannot be used unequivocally. The above effect was examined by the electron probe.

X-ray diffraction patterns were made of the 2% magnesia-containing composition at 1550 and 1750°C and the presence of spinel was substantiated. Since spinel is detected, the percentage of spinel present can be estimated at approximately 5 to 10%.

The theoretical density of the 2% magnesia-containing composition was determined by optical microscopy methods to be 3.96 g/cc. Since a comparison of sintering data made on the basis of bulk density is invalid when the theoretical densities of the compositions are different, this determination was critical.

Grain size determinations indicate that grain size was not a function of composition at 1550°C. Jergensen reported a difference in grain size of 0.1 micron at this temperature with compositions containing 0.0% and 0.1% MgO-containing compositions (Ref. 34). Due to both the inherent meaning of the term "average grain size" and the experimental error, it is felt that differences in grain size of this order are not significant. Jergensen then proceeded to utilize this information to explain the effect of magnesia in the sintering of alumina. The results reported herein appear to be more conclusive and possibly of greater significance. From Bruch's studies (Ref. 35), Jergensen has shown that the pure alumina specimens were contaminated by magnesia. This occurred because of magnesia's volatility during firing. Therefore differences in grain size between a 1/4% magnesia-containing composition and the pure alumina composition were not reported by Coble (Ref. 36). In the effort reported herein samples were placed in covered impervious alumina crucibles during the firing operation. It therefore seems unlikely that sufficient magnesia could be introduced to the pure alumina composition to cause the grain size effect noted by Jergensen. In his experiment it must have been necessary to fire the composition in different furnaces. Even if it is assumed that a grain size difference of 0.1 micron is significant, it seems that variations in grain size due to time, temperature and temperature distribution might easily account for the observed difference. If sufficient magnesia evaporated and diffused from the magnesia-containing composition to the pure alumina composition and also resulted in a similar grain size for both compositions, then these compositions would be fairly similar and should have similar sintering rates. This was not observed by Jergensen. It is felt that even though a mechanism of grain growth inhibition would yield different sintering rates, the actual mechanism is one of the formation of both a solid solution and solid solution gradient of magnesia in alumina. If the mechanism of this solid solution is partially or wholly the replacement of $2Al^{+3}$ by $2Mg^{+2}$ and creation of an oxygen vacancy, an increased vacancy concentration and concentration gradient would result. This increased vacancy concentration and vacancy gradient would be in the proper direction to enhance the sintering rate.

In an attempt to prove the mechanism postulated above, the solid solution and solid solution gradient of magnesia in alumina, the back-reflection x-ray camera and electron microprobe analyzer were used.

The results obtained with the back-reflection x-ray camera using both Linde A starting material and the pure alumina composition were compared to the 1/4% magnesia-containing composition and showed no indication of solid solution. This result differs from Jergensen's. The change in d-spacing reported by Jergensen seems excessive. If a change in d-spacing of the order of magnitude shown by Jergensen exists, it would have been observed by these authors. The results obtained in this study using the back-reflection camera can be interpreted to mean one of the following:

1) No solid solution exists.
2) Little if any change in d-spacing would be noted when the solid solution is partly or wholly interstitial.
3) The magnesia concentration was too low for detection.
4) If a solid solution gradient exists, this technique will measure an average value which would be far less than a uniform magnesia distribution. Therefore, the solid solution would be even more difficult to detect.

The electron probe analyzer was used to clarify the mechanism by which magnesia affects the sintering kinetics of alumina. The following results obtained with the electron probe will show why the back-reflection camera technique was unsuccessful.

The results obtained from the electron probe indicate the following:

1) Every area examined, including the sample whose Mg fluorescent picture was black, had some magnesia. Only a few localized regions gave some isolated values of 0% Mg.
2) Regions designated as spinel grains were found containing 3 to 4 wt. % Mg in areas containing one or a few grains at 1750°C.
3) A solid solution gradient of magnesia in spinel occurs at 1750°C.
4) Segregation of Mg in localized regions forming spinel crystals of similar size to the best grain size were noted at 1750°C but not at 1550°C.
5) The limit of solid solution of magnesia in alumina was postulated to vary from 0.1% to 0.008% Mg by weight.
6) A possible solid solution gradient of magnesia in alumina was determined.

In order to interpret the sintering results, some of the probe results will be discussed.

It was observed from the sintering results that the sintering rate was not a function of magnesia content above a certain critical level. This can be interpreted to indicate that spinel above certain concentrations does not affect the sintering of alumina. If the low-temperature and high-temperature data are compared, a small compositional effect may exist at 1550°C. Since the composition of the spinel phase increases in alumina content with increasing temperature, producing a probable decrease in theoretical density (spinel is less dense than alumina) with increasing temperature, this effect probably accounts for the slight difference in sintering rate of magnesia-containing compositions. As

further evidence in support of the similar sintering rates of magnesia-containing compositions, there is a large degree of similarity in magnesia distribution up to the point of spinel formation between the 0. 1/4 and 2.0% magnesia-containing samples as determined by optical microscopy and electron probe analysis. Variations noted in the magnesia content of the specimen were indicated. However, these variations were of total quantity rather than the manner of distribution.

A probable solid solution and a solid solution gradient were detected at high temperatures with the magnesia-containing compositions. A segregation of spinel into large localized regions was observed at 1750°C. This segregation may be due to either localized magnesia concentrations which were noted to a slight extent at 1550°C with the electron probe, or to incompatibility (high interfacial energy) between spinel and alumina.

The probable solid solution and solid solution gradient can only be justified at 1750°C, since at 1550°C the grain size was generally too small for interpretation with the electron probe. Total porosity studies indicate the similarity in relative sintering rates of the magnesia-containing compositions and the pure alumina composition at both 1550 and 1750°C. The rate of normal grain growth was compositionally insensitive and exaggerated grain growth did not occur in any composition in vacuum or hydrogen at 1550°C. Therefore the enhanced rate with magnesia additions cannot be a function of either normal or exaggerated grain growth.

As a result of the above, a solid solution and/or a solid solution gradient of magnesia in alumina may be theorized at 1550°C. The solid solution formed is probably temperature-sensitive and should increase with increasing temperature.

If the solid solution is partially the replacement of $2Al^{+3}$ by $2Mg^{+2}$, then an increase in both the diffusion coefficient and the vacancy concentration gradient will produce an enhanced sintering rate. Electron probe and sintering results show that the solid solution mechanism of magnesia in alumina is probably predominantly substitutional rather than interstitial. A minimal effect or a decrease in sintering rate should result, since excess vacancies should not be generated with an interstitial solid solution. This decrease or minimal effect is contrary to the observed results. Fick's Law shows that the multiplication of the diffusion coefficient by the concentration gradient yields the rate of mass transfer by diffusion. The effect of magnesia can now be explained by recognizing that the probable solid solution and solid solution gradient formed can increase either the diffusion coefficient or the vacancy concentration gradient or both, and thereby increase the sintering rate. It is still necessary to prove conclusively that magnesia in solid solution with alumina will produce vacancies.

Jorgensen (Ref. 34) and Cutler (Ref. 37) showed that magnesia acts as a sintering inhibitor to alumina in the initial stages of sintering at about 1300°C. Jorgensen stated that this inhibition was due to a reduction of the diffusion coefficient by a solid solution mechanism near the grain boundary. He assumed that the measurements he had made at 1830°C which determined the solid solution of magnesia in alumina in the vicinity of the grain boundary were applicable at 1300°C. He then showed experimentally that magnesia could reduce the sintering rate of alumina and reported that this change was due to a reduction of the diffusion coefficient.

Two possibilities for their conclusions are proposed:

1) a change in type of solid solution with temperature.
2) the effect of spinel on the sintering rate of alumina at low temperatures.

In the first case, if it is assumed that solid solution occurs at 1300°C, the type of solid solution may be totally or partially interstitial. As the temperature is raised, the nature of this solid solution may change, i. e., larger percentages of a one for one replacement of Al^{+3} by Mg^{+2} may occur, thereby enhancing the sintering rate. In the second case, the solid solution of magnesia in alumina may not exist and the effect observed could be due only to spinel. From the calculations made previously on Navias' work (Ref. 38), there seems to be small likelihood that magnesia would diffuse from the spinel formed at 1300°C into the alumina grains. At temperatures near or above 1550°C, aluminum and magnesium are sufficiently mobile to form some solid solution of magnesia in alumina. The mechanism of spinel's inhibition of the sintering of alumina may be due to either a lowering of the surface energy or a lowering of the diffusion coefficient in the manner shown below.

As indicated by the microstructural results at 1550°C, a spinel second phase was noted as a coating or a fine dispersion at the grain boundary. The path of diffusion of a vacancy in this system would begin at the spinel layer and diffuse through both this layer and the alumina grain to the grain boundary, where it is finally eliminated. This process may lower the diffusion coefficient. As the temperature is raised above 1300°C, an increasing percentage of magnesia enters the alumina grains as a solid solution. A gradient of magnesia concentration is built into the alumina grains. The effects of both the solid solution and the gradient overshadow the inhibiting effect of spinel. This results in an enhanced sintering rate. The enhanced sintering rate of compositions containing magnesia has been shown by this investigation in the temperature region of 1550 to 1750°C. Similar sintering rates of all magnesia-containing compositions indicate that the spinel phase, at least at higher concentrations, is relatively unimportant in sintering in this system. This independence tends to agree with the mechanism just proposed.

E. Conclusions

1. Minimum Conditions for Attaining 99% of True Density

Temperature	Time	Atmosphere	Magnesia Addition
1550°C	3 hrs	Vacuum	2%
1550°C	7 hrs	Vacuum	1/4%
1650°C	1 hr	Hydrogen	1/4+2%
1650°C	4 hrs	Helium	1/4+2%

2. Minimum Conditions for Attaining 100% of True Density

Temperature	Time	Atmosphere	Magnesia Addition
1750°C	1 hr	Vacuum and hydrogen	1/4%
1750°C	3 hrs	Vacuum and hydrogen	2%

100% alumina exhibits 1.9% porosity at best.

3. Atmospheric Effects

a) The sintering rate was found to be independent of firing atmosphere at high temperatures with either hydrogen or vacuum, which indicates the probable diffusion of hydrogen as H° or H^{+}.

b) There was no indication that hydrogen enhances the sintering rate of alumina by creating lattice defects.

c) At low temperatures the sintering rate was affected by gas diffusion through the pores. The higher the diffusivity of the gas the higher the sintering rate.

d) The initial sintering rate in helium was higher than hydrogen at 1550°C, but decreased with decreasing open porosity.

e) Over-firing was observed to occur as a function of both time and temperature in helium at higher temperatures

f) Theoretical density was reached only in vacuum and hydrogen.

g) Normal grain growth was not a function of firing atmosphere.

h) Exaggerated grain growth occurred with the pure alumina composition in vacuum, hydrogen and helium.

i) Exaggerated grain growth occurred at a lower temperature in helium with the pure alumina composition than in vacuum or hydrogen.

j) No exaggerated grain growth occurred with the magnesia-containing samples in vacuum or hydrogen.

k) Significant amounts of exaggerated grain growth occurred with the 1/4% magnesia composition in helium at 1750°C. Little indication of exaggerated grain growth was found for the higher magnesia-containing compositions.

4. Effects of Magnesia Additions

a) The pure alumina composition had a lower sintering rate than the magnesia-containing compositions.

b) At 1550°C the rate of normal grain growth was independent of composition in hydrogen or vacuum.

c) The mechanism proposed for the enhanced sintering rate with additions of magnesia is the formation of a solid solution and a solid solution gradient that probably increase the diffusion coefficient and the vacancy concentration gradient.

1) The only mechanism of solid solution that seems to yield results in agreement with these obtained is the replacement of $2Al^{+3}$ by $2Mg^{+2}$ and the creation of an oxygen vacancy. Other types of solid solution mechanisms proposed seem to decrease or have little effect on the number of vacancies.

d) The activation energy for vacancy movement could not be measured.

e) The activation energy for sintering in the intermediate and final stage of sintering could not be measured.

f) No dislocations were seen with the limited number of samples investigated (dislocation densities of 10^{5} normally found in alumina would correspond to from 1 to .1 or less dislocations per field of view) with the electron microscope. This would tend to indicate, in a limited manner, that dislocations have little effect on sintering. This agrees with the sintering literature on alumina.

g) No observable difference was noted in the manner in which spinel was distributed in all magnesia-containing compositions by both the optical microscope and electron probe analysis.

h) Using optical microscopy methods, spinel was found as a coating or as a dispersion of small crystals along the alumina grain boundaries at 1550°C.

i) A segregation of spinel was found at 1750°C.

j) Spinel was formed as irregularly shaped grains and in cubes between alumina grains at 1750°C.

k) X-ray diffraction indicates the formation of spinel at 1550 and 1750°C with the 2% magnesia-containing sample.

l) The segregation of spinel at 1750°C indicates incompatibility (high interfacial energy) between alumina and spinel and/or local inhomogeneities.

m) The theoretical density of the 2% magnesia-containing composition was found to be 3.96 g/cc at 1750°C. This value may change as a function of temperature due to the variation in the alumina content of the spinel solid solution.

n) Solid solution of magnesia in alumina was not found with the back-reflection x-ray camera.

o) When using the back-reflection x-ray camera, no variation in d-spacing was observed as a function of both grain size and temperature with the 1/4% magnesia-doped composition.

p) Electron microprobe analysis:

1) Except for a few isolated points, all areas examined had some measurable percentage of magnesium.

2) Spinel grains were found and a solid solution gradient of Mg increasing from the grain boundary to the interior was observed.

3) Magnesium was found to be segregated at 1750°C but not at 1550°C.

4) A probable solid solution of magnesia in alumina is theorized which varies from about 0.1% Mg to 0.008% Mg at 1750°C. This solid solution was inferred to exist at 1550°C from experimental results. Further studies are needed because some conflicting data were obtained.

5) If a solid solution exists, then a solid solution gradient of magnesia in alumina was found with magnesia increasing in concentration as the grain boundary is approached at 1750°C. This gradient was also inferred at 1550°C from experimental measurements.

6) A large degree of similarity was found between the magnesia-containing compositions. This result tends to substantiate the similarity in sintering rates found with the magnesia-containing compositions.

7) Two proposed mechanisms were postulated to explain (i) the inhibition of sintering of alumina by magnesia during the initial stage of sintering, and (ii) the enhanced rate found during the intermediate and final stages of sintering of alumina. They are:

   i) With increasing temperature, the mechanism (type of solid solution) of solid solution of magnesia in alumina may change from mostly interstitial to most substitutional.

   ii) If solid solution of magnesia in alumina is non-existent during the initial stage of sintering, spinel may act to inhibit the sintering of alumina by reducing the surface energy and/or the diffusion coefficient. Then as the temperature is raised, magnesia enters the alumina structure in solid solution and overshadows the effect of spinel in the intermediate and final stages of sintering.

III. Devitrification Studies

A. Introduction

This third phase of the research program deals with the development of ceramic bodies which mature in the 1800 to 2600°F temperature range. The devitrification approach of the prereacted raw materials technique has been utilized in the fabrication of these compositions. This technique resulted in significant improvement over conventional fabrication in at least three areas. Excellent reproducibility of samples can be attained, since the raw materials are mixed on an atomic basis in the fritting operation. Secondly, the quenched glass can be ground easily to the desired particle size for optimum packing, and thirdly, the crystal size of the final body may be controlled with proper heat treatment. The basic steps in the fabrication are as follows: melting of the total composition, quenching in water drying, grinding to a controlled particle size distribution, fabrication into specimens, and firing. In the firing operation, a crystalline phase is devitrified from the glass. Thus the resulting body is then a matured crystalline body containing some glass for densification.

Compositions containing cordierite,* $2MgO \cdot 2Al_2O_3 \cdot 5SiO_2$, as the major crystalline phase were selected for the study. The stable high temperature polymorph of cordierite, the alpha form, is characterized by a low coefficient of linear thermal expansion, approximately 1.3×10^{-6} in/in/°C over the temperature range 25° to 700°C. This low thermal expansion is conducive to high thermal shock resistance, which is a primary requirement in the development of radome materials.

A serious disadvantage of most cordierite compositions prepared conventionally, that is, by solid phase reaction, is the narrow firing range. In order to increase the firing range, commercial bodies are chosen with a composition significantly removed from the theoretical cordierite composition in order to develop a liquid phase which results in densification. However, these compositions contain a substantial amount of other crystalline phases, and with the glass present, exhibit increased thermal expansion and thus reduced thermal shock properties. If a composition of theoretical cordierite is utilized, the liquid phase necessary to densify the body can only come from the incongruent melting of the phase. This is unsatisfactory owing to the rapid nature of the melting and to low viscosity of the glass formed. Whether pure cordierite can be sintered has not been determined.

With the fabrication of a cordierite body, two factors must be considered: (1) maximum cordierite development for low thermal expansion, and (2) sufficient liquid phase to densify the body without adversely affecting the amount or development of the cordierite phase. The addition of the liquid phase may be approached from two aspects. The first is the melting of a composition near the cordierite composition, such that cordierite and another phase, glass and/or crystalline, would be developed. These other phases would react with the cordierite to form a liquid phase below the incongruent melting temperature of the cordierite, thus preserving sufficient cordierite to dominate the expansion characteristics of the body. The second approach deals with the incorporation of a second frit which would supply the glass phase necessary for densification of the cordierite pro-

*Complete literature survey in Report No. 3, NOw 64-0040-d.

duced from a pure cordierite glass. In this manner, it would not be necessary for the cordierite development to be inhibited by reactions to form a liquid phase.

In the previous Naval Contract NOw 64-0040-d, a preliminary study of cordierite compositions was conducted utilizing both the one-frit and two-frit approaches. Two compositions out of eighteen one-frit compositions were found to attain maturity and possess a low thermal expansion. The initial two-frit composition developed possessed low thermal expansion and an extended firing range.

B. Program of Study

This present work deals with an extension of the principle developed in the earlier contract. The one-frit compositions were evaluated with regard to density, moisture absorption, firing temperature, linear thermal expansion, electrical properties, transverse strength, and microstructure. The two-frit compositions developed were evaluated for the same physical properties. Also, nine glasses were studied as densifying glasses or the second glass for the two-frit system for the cordierite compositions. All of these were evaluated for thermal expansion, and all were evaluated for firing range, density, moisture absorption, crystalline phases present, in 10%, 20% and 30% additions to the base pure cordierite glass, which is the glass which produces the principal crystalline phase in the two-glass system.

C. Compositions

Figure 15 shows the location and several properties of compositions studied on the $MgO \cdot Al_2O_3 \cdot SiO_2$ equilibrium diagram. Most of this information is from the last contract and the details are reported in the last Final Report. This information serves as reference and background information with respect to the one-glass approach to the devitrification technique. Table III lists the composition

Table III

COMPOSITIONS EVALUATED IN THE $MgO \cdot Al_2O_3 \cdot SiO_2$ SYSTEM

	C-8	C-13	Co	Cb-9	Cb-98	Cb-910	Cb-96
SiO_2	52	55	51.4	58.0	52	55	61.4
MgO	25	10	13.7	7.67	8.3	6.67	6.4
Al_2O_3	23	35	34.9	19.0	23	25	18.3
BaO				7.67	8.3	6.67	6.4
CaO				7.67	8.3	6.67	6.4

	C-A	C-B	C-C	C-D	C-E	C-F
SiO_2	58	55	55	61	61	49
MgO	6.67	8.67	7.67	8.67	3.69	8.67
Al_2O_3	22	19	22	13	25	25
BaO	6.67	8.67	7.67	8.67	3.67	8.67
CaO	6.67	8.67	7.67	8.67	3.67	8.67

Code
Composition #
Coefficient of Linear Thermal Expansion (x 10^{-6})
Moisture Absorption (%)

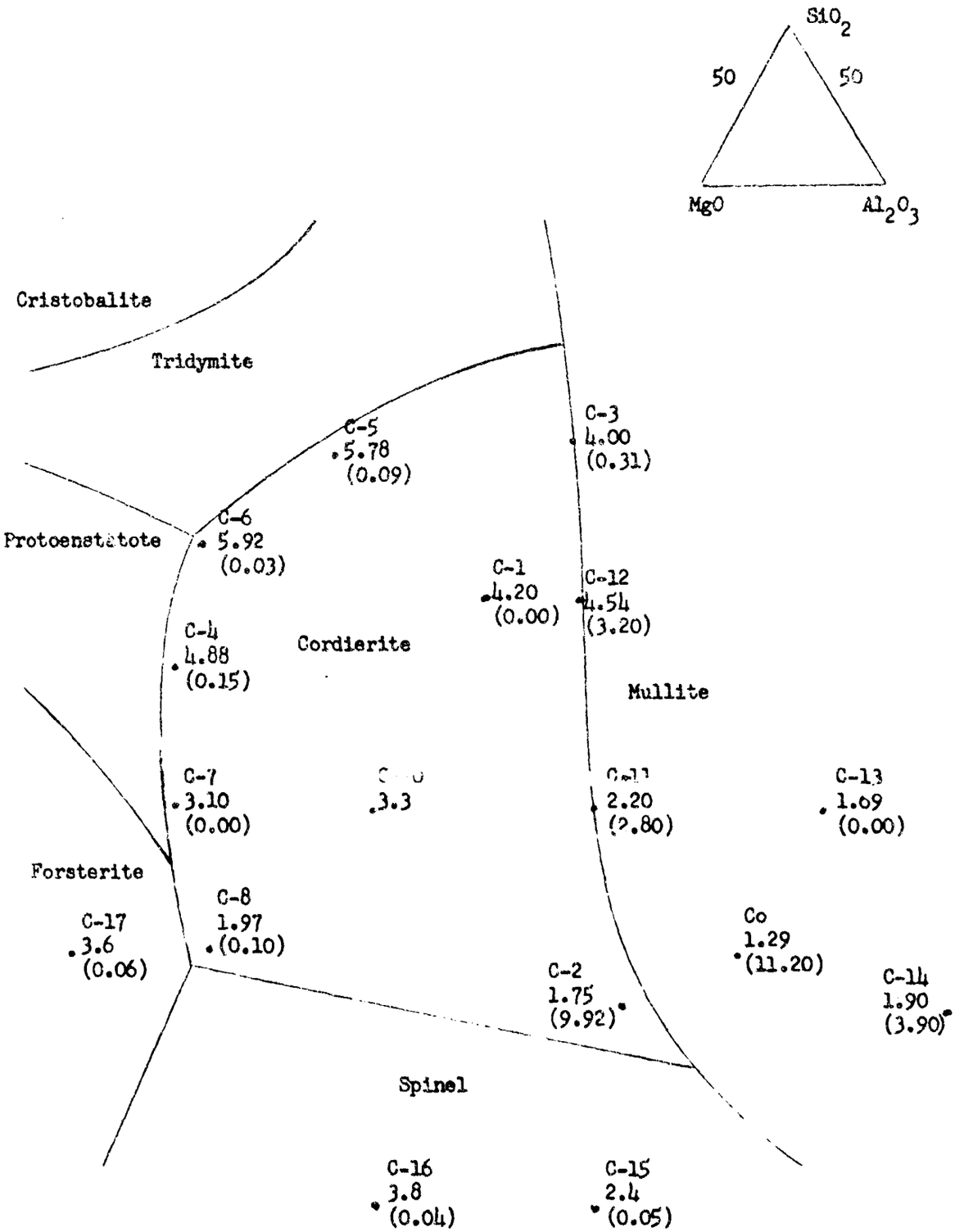

Fig. 15--Properties of Compositions Evaluated in the $MgO \cdot Al_2O_3 \cdot SiO_2$ System

of several pertinent compositions from Fig. 15 along with those of the fluxing or low melting glass which will be added to the cordierite or second glass. Figure 16 shows the location of the compositions in the $RO \cdot Al_2O_3 \cdot SiO_2$ system, in which RO represents MgO, CaO and BaO, which are added as carbonates; the alumina and silica were added as oxides.

D. Processing Procedures

All compositions were weighed and then mixed in a twin shell blender for 1 hour. In order to decrease the bulk all $Al_2O_3 \cdot SiO_2 \cdot MgO$ compositions were calcined to 1800°F, and all $Al_2O_3 \cdot SiO_2 \cdot MgO \cdot BaO \cdot CaO$ compositions were calcined to 1500°F. Each batch was then passed through a -200 mesh screen to break up agglomerants. The compositions were then melted individually in fire clay crucibles in a gas-fired pot furnace, quenched in water, dried, and milled dry for 48 hours in an alumina mill with alumina pebbles. This ground material was then passed through a -200 mesh screen, and was used as the raw material in fabrication.

In the one-frit compositions, the raw material was mixed with 5% of a 5% Superloid solution, and pressed at 15,000 psi into 1" diameter flat discs. These discs were fired to the appropriate maturing temperature in 6 hours plus a 1-hour soaking period.

In the two-frit compositions, the two frits were weighed out in the correct proportions and wet-milled for 24 hours in alumina mills with alumina pebbles, using ethanol as the fluid phase. Discs of the same size as noted above were pressed under the same conditions, using 5% by weight of a 5% Superloid solution as a binder. These discs were then fired to the appropriate maturing temperatures in 6 hours plus a 1-hour soaking period.

E. Results

1. One-Frit Approach

In the previous Naval Contract, NOw 64-0040-d, 18 compositions were prepared utilizing the devitrification technique. These compositions were evaluated with regard to thermal expansion, density, moisture absorption, and firing range. Figure 16 shows their compositional locations in the phase diagram, along with their thermal expansions, and minimum moisture absorptions. The object was to develop a body with a low thermal expansion, zero moisture absorption, and at least a 25°F firing range. Two compositions, C-8 and C-13, were the only compositions which satisfied these requirements. The composition and fritting temperature of these bodies are shown on Table IV along with their physical properties.

These two compositions were prepared in larger batches in order to evaluate more fully the physical properties. Table IV presents the maximum density, minimum moisture absorption, firing temperature and range, coefficient of linear thermal expansion, electrical properties, transverse strength, grain size, and crystalline phases present.

As can be seen from Table IV, both bodies exhibit relatively high densities, zero or almost zero moisture absorption, at least a 25°F firing range, and coefficients of linear thermal expansions below 1.97×10^{-6} in/in/°C. The transverse strength of C-13, 15,000 psi, is in the upper range of values for cordierite com-

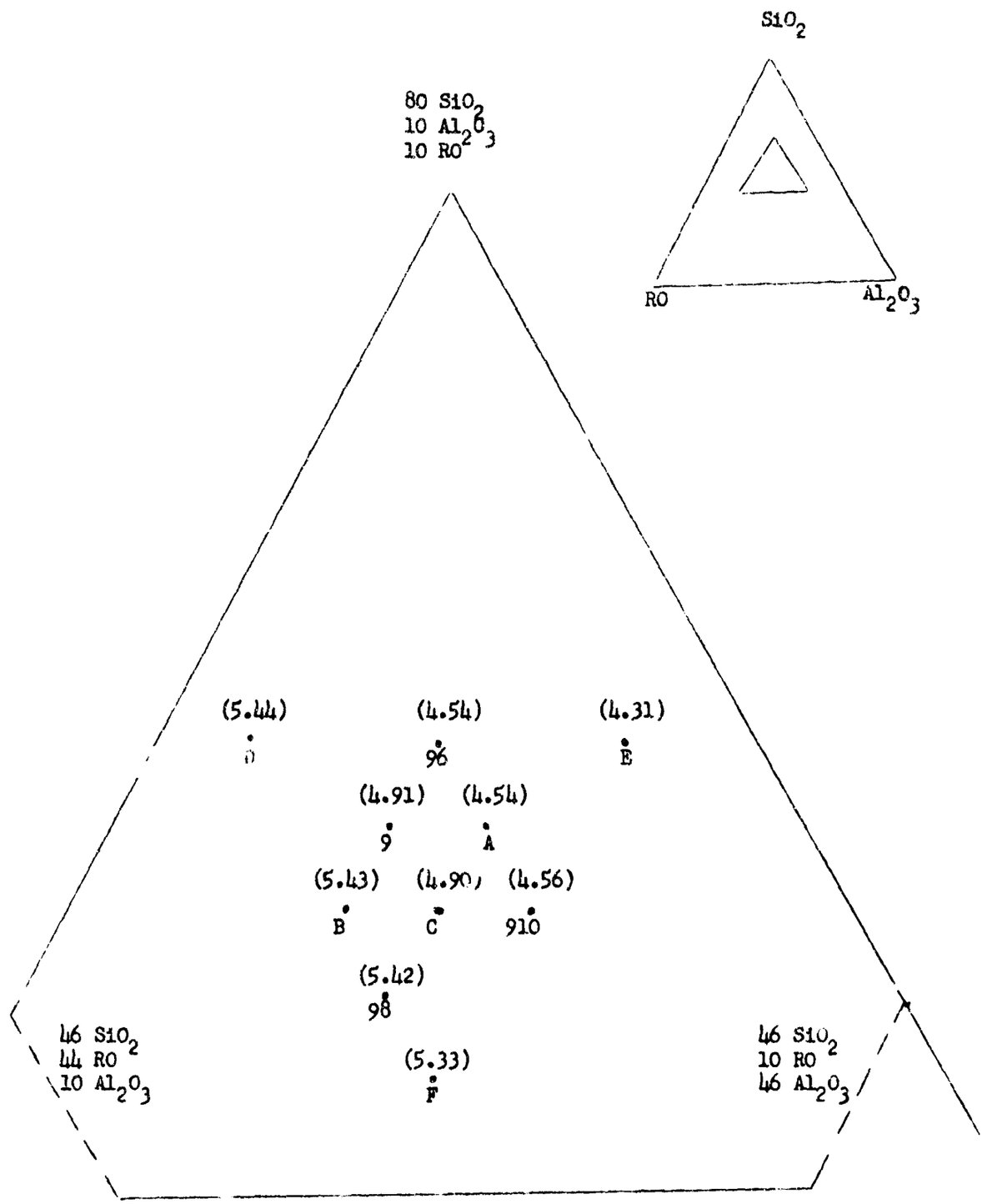

Fig. 16--Thermal Expansion of Low Melting Glasses in the $RO \cdot Al_2O_3 \cdot SiO_2$ System

Table IV

PROPERTIES OF THE ONE-FRIT TYPE COMPOSITIONS

	C-13	C-8
SiO_2 (%)	52	55
Al_2O_3 (%)	23	35
MgO (%)	25	10
Fritting Temperature (°F)	2600	2780
Density (g/cc)	2.45	2.41
Moisture Absorption (%)	0.00	0.10
Firing Temperature (°F)	2600	2525
Coefficient of Linear Expansion ($\times 10^{-6}$ in/in/°C)	1.69	1.97
Dielectric Constant	5.45	5.45
Power Factor (%)	0.21	0.29
Loss Factor (%)	1.16	1.60
Transverse Strength (psi)	15,000	13,300
Grain Size (μ)	3-7	3-7
Firing Range (°F)	2580-2610	2510-2535
Crystalline Phases Present	Cordierite Mullite (minor)	Cordierite Fosterite (minor)

positions. Microscopic studies show the grain size to be 3-7 microns with an evenly distributed glassy bonding phase, and approximately 7% closed void space. The electrical properties show average dielectric constants for cordierite compositions, and power factor and loss factor are in the range expected from this type of body.

Over-all, both bodies possess desirable physical properties, low thermal expansion, relatively high strength, and a workable firing range. With minimum additional effort, both compositions should perform adequately for radome applications.

2. Two-Frit Approach

In the previous Naval Contract, NOw 64-0040-d, cordierite compositions were studied in which additions of a low melting, devitrifiable glass were made to a cordierite glass in order to maximize cordierite development, extend the firing range, and to mature the body. Only one glass, Cb-9, was added to the cordierite glass, Co, in 10%, 20% and 25% additions. Low expansion bodies with an extended firing range were realized.

The first phase of the present study deals with a more complete evaluation

of the physical properties of the Co-Cb-9 compositions. These bodies were evaluated with regard to density, moisture absorption, firing temperature range, coefficient of linear thermal expansion, electrical properties, loss of weight in water, crystalline phases present, and microstructure.

The second phase of this effort deals with the development of other low melting frits to be added to the cordierite frit. Nine other glasses were prepared and evaluated with regard to firing range and thermal expansion values.

a. Co-Cb-9 Frit. Evaluation of Physical Properties

The evaluation of the physical properties for 10%, 20% and 25% additions of Cb-9 to the cordierite glass, Co, are shown in Table V. It can be seen that all bodies have 0.00% moisture absorption, relatively high densities, a firing range from 50°F for a 10% Cb-9 addition to 150° for a 25% addition, and low thermal expansions, 1.55 x 10^{-6} in/in/°C for a 10% Cb-9 addition up to 1.99 x 10^{-6} in/in/°C for a 25% addition. A study of the microstructure shows grains the 2-10 μ range with a void content approximately 7% of volume. The electrical properties of the 20% Cb-9 additions show the body to be in the L3 grade range of the MIL 1-10 Specification.

b. Evaluation of Individual Densifying Glasses

i. Firing Range

Table VI shows the change in density and moisture absorption with regard to temperature. While the actual densification temperatures vary slightly, it can be seen that all compositions have a 400°F firing range over which the density changes only slightly, and the bodies remain non-porous. In all cases except C-E, the compositions are non-porous at 1800°F and melted at 2300°F.

Figure 16 shows the compositional points in a ternary $SiO_2 \cdot Al_2O_3 \cdot RO$, where RO is equal molar portions of MgO, BaO and CaO. It can be seen that there is no correlation between compositional points, extended firing ranges, and high densities. Generally the highest densities and longest firing ranges are found for bodies C-B, C-C, Cb-9 and C-F, which are in the center of the diagram.

ii. Differential Thermal Analysis

Differential thermal analysis was performed on the glasses Co, Cb-9, Cb-98, Cb-96 and Cb-910. The curves are shown in Fig. 17. The curves of Cb-98, Cb-9, Cb-96 and Cb-910 possess similar shapes with regard to temperature; thus only one representation is needed for these glasses.

The differential thermal analysis of the Co glass is interpreted as follows: there is no reaction until 780°C, at which temperature the glass begins to nucleate; nucleation continues to about 936°C, at which temperature the glass crystallizes into μ-cordierite, then at 970°C transforms into cordierite, and above 1000°C grain growth is occurring.

The differential thermal analysis of the Cb-9 type of glasses is seen to be significantly different. There is no reaction until 732°C, at which temperature nucleation occurs; above 840°C, two things are occurring: the glass is softening and crystallization is taking place. The endothermic reaction associated with

Table V

PHYSICAL PROPERTIES OF TWO-FRIT BODIES

	90% Co 10% Cb-9	80% Co 20% Cb-9	75% Co 25% Cb-9
Density (g/cc)	2.37	2.25	2.24
Moisture Absorption (%)	0.00	0.00	0.00
Firing Range (^{o}F)	50 (2575-2625)	75 (2500-2575)	100 (2450-2550)
Coefficient of Linear Thermal Expansion ($\times 10^{-6}$ in/in/^{o}C)	1.55	1.83	1.99
Loss of Weight in Water (%)	0.0	0.0	0.0
Dielectric Constant		4.75	
Power Factor (%)		0.30	
Loss Factor (%)		1.43	
Transverse Strength (psi)	13,000	11,500	
Crystalline Phases Present	Cordierite	Cordierite	Cordierite
Grain Size (μ)	2-10	2-10	2-10
Firing Temperature (^{o}F) (Specimens Tested)	2600	2550	2500
Void Content (%)	7	7	7

Table VI

MOISTURE ABSORPTION (%) vs. FIRING TEMPERATURE (^{o}F)

	C-A	C-B	C-C	C-D	C-E	C-F	Cb-98	Cb-910	Cb-96	Cb-9
1500	1.73	1.57	1.55	1.92	1.44	1.60	-	-	-	-
1600	1.76	2.16	1.89	2.59	1.45	2.17	2.73	2.55	2.59	2.59
1700	2.23	2.73	2.72	2.72	1.75	2.80	2.75	2.65	2.60	2.67
1800	2.65	2.83	2.77	2.75	2.63	2.85	2.67	2.65	2.74	2.74
1900	2.66	2.82	2.79	2.77	2.67	2.84	2.73	2.67	2.68	2.74
2000	2.67	2.83	2.83	2.75	2.67	2.84	2.72	2.65	2.64	2.73
2100	2.68	2.83	2.85	2.72	2.68	2.85	2.70	2.63	-	2.72
					2.58	2.69	2.65			2.52
2200	2.67	2.83	2.79	melted	2.56	2.57	2.46			
2250	2.58	2.82	2.77							
2300	melted	melted	melted			melted	melted	melted	melted	melted
1500	16.00	21.28	21.64	12.64	24.46	21.47	-	-	-	-
1600	15.90	9.11	14.10	1.28	24.05	9.47	.02	1.08	.05	.00
1700	6.6	0.0	0.0	0.0	16.30	0.0	.00	.00	.00	.00
1800	0.0	0.0	0.0	0.0	0.0	0.0	.00	.00	.00	.00
1900	0.0	0.0	0.0	0.0	0.0	0.0	.00	.00	.00	.00
2000	0.0	0.0	0.0	0.0	0.0	0.0	.00	.00	-	.00
2100	0.0	0.0	0.0	0.0	0.0	0.0				
2200	0.0	0.0	0.0	-	0.0	0.0	.00	-	-	.00
2250	0.0	0.0	0.0	0.0	-	0.0	.00	-	-	.00

Fig. 17--Differential Thermal Analysis of a Low Melting Glass and Cordierite Glass

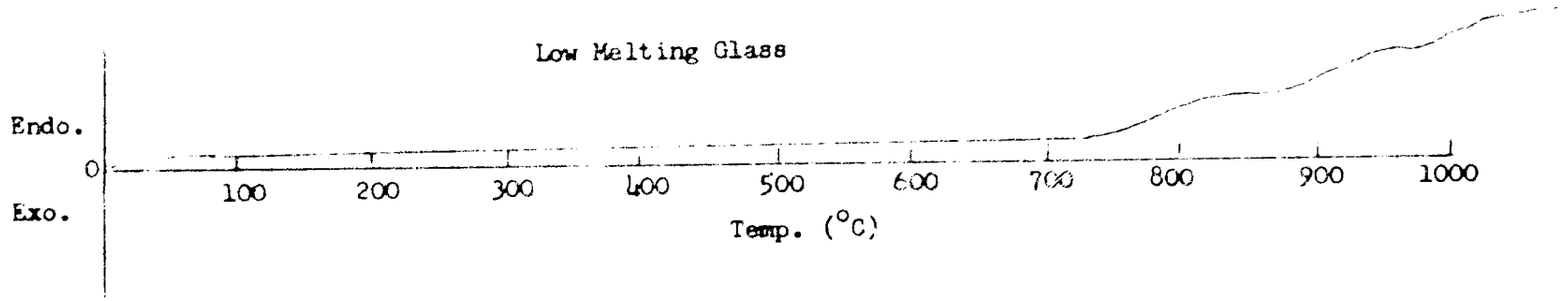

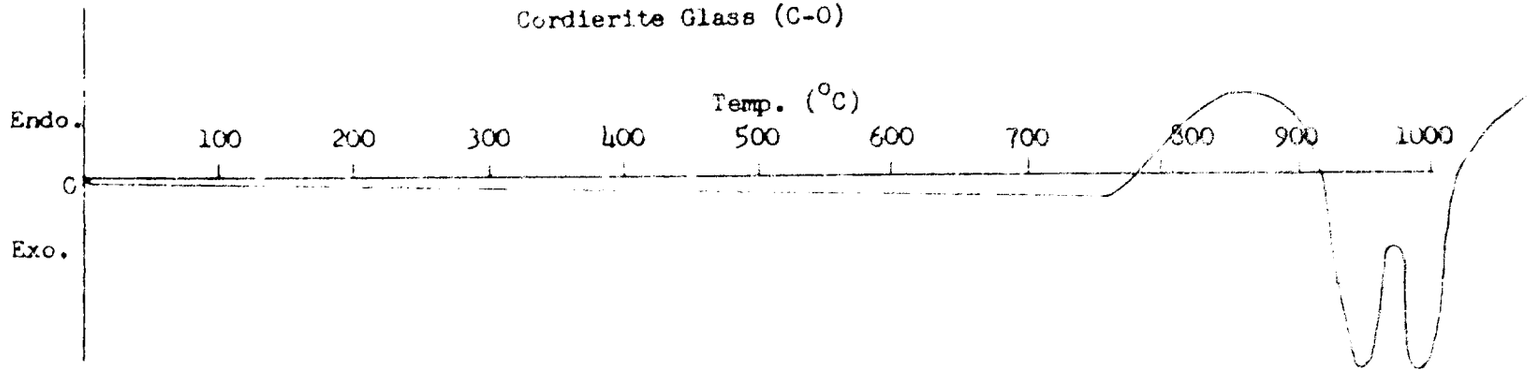

Table VII

CRYSTALLINE PHASES PRESENT

Co	Cordierite	
Cb-9	BaC[#]	Unknown[◇]
Cb-98	BaC	Unknown
Cb-910	BaC	Unknown
Cb-96	BaC	Unknown
C-A	BaC	Unknown
C-B	BaC	Unknown
C-C	BaC	Unknown
C-D	BaC	Unknown
C-E	BaC	Unknown
C-F	BaC	Unknown
C-8	Cordierite	(Fosterite)[*]
C-13	Cordierite	(Mullite)[*]

[#] $BaO \cdot MgO \cdot Al_2O_3 \cdot SiO_2$ phase reported by H. R. Wisely, "Phases in the Ternary System $BaO \cdot MgO \cdot Al_2O_3 \cdot SiO_2$," Ph. D. thesis, Rutgers, 1952.

[◇] Peaks at 22.0, 25.8, 28.0, 29.6, 36.9°. Others may be masked by BaC.

[*] Minor phase.

softening masks the crystallization peaks. Crystallization was found to occur in this temperature range by x-ray analysis.

iii. X-Ray Analysis

All glasses were heated to above their crystallization temperatures, 2250°F, and then analyzed for crystalline phases present, using standard x-ray diffraction techniques. The phases present are shown in Table VII above.

As can be seen from this table, all the densifying glasses devitrify into BaC and an unknown phase. BaC was formed and investigated by Wisely at Rutgers in 1952.

As was expected, cordierite is the only phase which devitrifies from the Co glass, and is the major phase in the C-13 and C-8 types of glasses. From their positions in the phase diagram, fosterite and mullite would be expected in C-8 and C-13 respectively.

iv. Thermal Expansion

The thermal expansions of Co, Cb-9, Cb-98, Cb910, Cb-96, C-A, C-B, C-C, C-D, C-E and C-F fired to 2600°F were determined utilizing a standard interferometer method. In the case of the low melting glasses, the material was placed in a platinum foil lined alumina crucible and melted at 2600°F. The coefficients of thermal expansion of specimens prepared from these compositions are shown in Table VIII and Fig. 18 shows the relationship between thermal expansion and composition.

Table VIII

COEFFICIENTS OF LINEAR THERMAL EXPANSION

OF FLUXING GLASSES

Cb-9	4.91
Cb-96	4.54
Cb-98	5.42
Cb-910	4.56
C-A	4.54
C-B	5.43
C-C	4.90
C-D	5.44
C-E	4.31
C-F	5.33

The ten glasses in the $Al_2O_3 \cdot SiO_2 \cdot MgO \cdot CaO \cdot BaO$ system were found to possess thermal expansions between 5.44×10^{-6} and 4.31×10^{-6}. From Fig. 18 it is seen that as the amount of RO elements is decreased, the thermal expansion decreases.

c. Evaluation of Combinations of Glasses

i. Firing Range

Table IX shows density and moisture absorption vs. firing temperature of compositions with 10, 20 and 30% additions of Cb-96, Cb-98, Cb-910, C-A, C-B, C-C, C-D, C-E and C-F to the base cordierite glass Co. It can be seen that as the percentage of low melting glass which is added to the cordierite glass increases, the firing range increases and the maturing temperature decreases. With a 30% addition, the maturing temperature is about 2450°F with a firing range from 2425°F to 2525°F. A 20% addition increases the maturing temperature to 2575°F with a firing from 2550°F to 2600°F. And a 10% addition increases the maturing temperature to 2625°F with a firing range from 2600°F to 2650°F. From a compositional standpoint, all additions appear to affect the density, moisture absorption and firing range in the same manner.

ii. Thermal Expansion

The coefficients of linear thermal expansions were determined from specimens fired to maximum density utilizing an interferometer. The expansion values of compositions containing cordierite glass with 10, 20 and 30% additions of Cb-9,

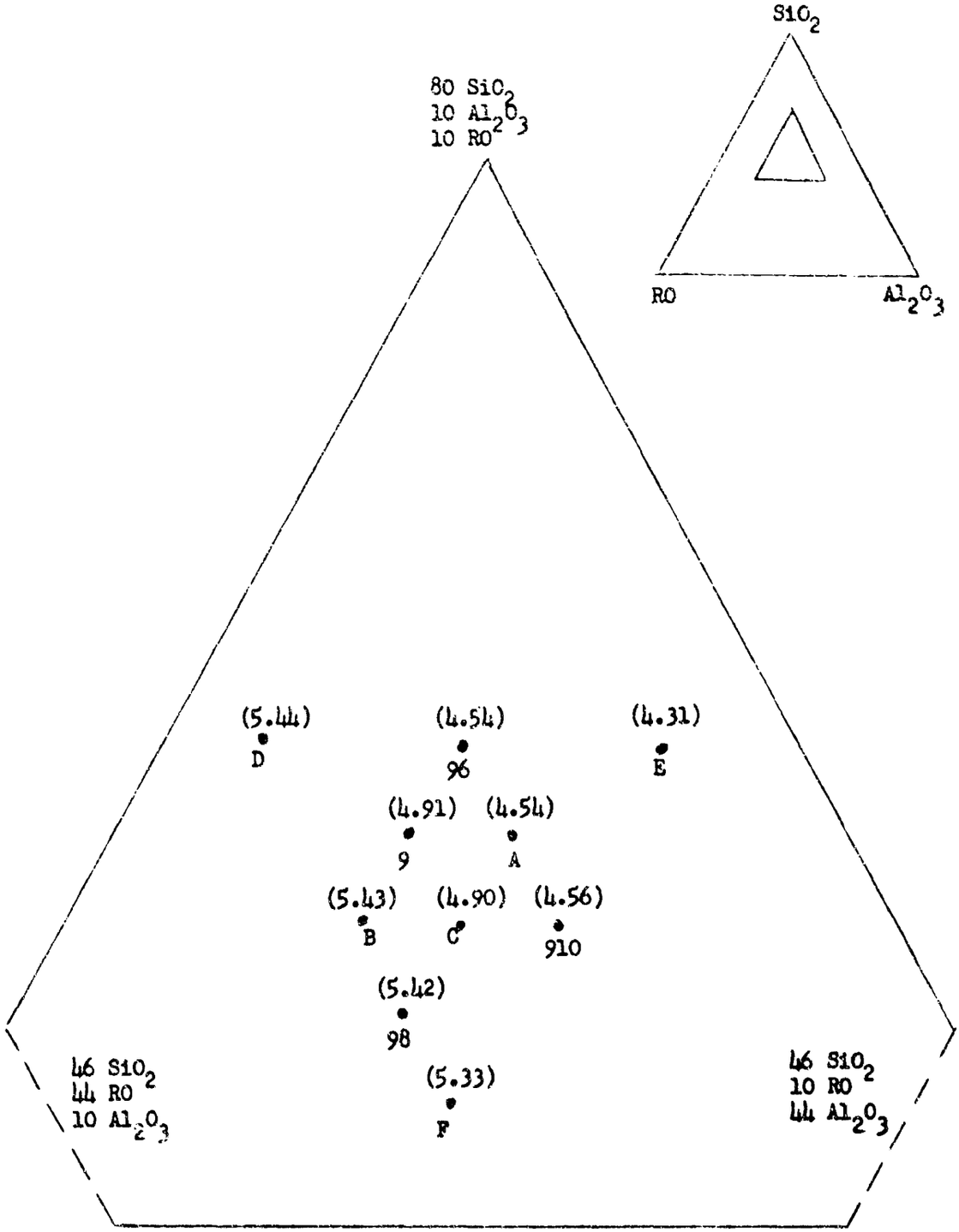

Fig. 18--Coefficients of Linear Thermal Expansion of Low Melting Glasses Studied in the $Ro \cdot Al_2O_3 \cdot SiO_2$ System

Table IX

DENSITY (g/cc) vs. FIRING TEMPERATURE (°F) AND

MOISTURE ABSORPTION (%) vs. FIRING TEMPERATURE (°F)

OF COMPOSITE BODIES

Fluxing Glass Content	Cb-98			Cb-96			Cb-910		
	30%	20%	10%	30%	20%	10%	30%	20%	10%
	Density (g/cc) vs. Firing Temperature (°F)								
2400	2.35	2.23	1.96	2.19	2.14	-	2.27	2.16	-
2425	2.36			2.23			2.28		
2450	2.34	2.26	2.16	2.26			2.29		
2475	2.33			2.26			2.29		
2500	2.35	2.28	2.18	2.30	2.17		2.38	2.25	
2525		2.36							
2550	2.14	2.42	2.24		2.31	2.10		2.42	2.19
2575		2.42	2.28		2.34	2.12		2.38	2.19
2600		2.34	2.34		2.44	2.41		2.44	2.27
2625			2.41			2.35			2.41
2650			2.36						2.42
	Moisture Absorption (%) vs. Firing Temperature (°F)								
2400	.22	1.07	9.44	1.19			0.42	4.25	
2425	.03			0.08			0.16		
2450	.00	.54	5.43	0.05			0.14		
2475	.05			0.10			.60		
2500	.03	.33	4.78	0.03	4.71		.21	2.10	
2525		.22							
2550	0.00	.00	2.55		0.25	5.71		0.08	1.58
2575		.12	.98		.61	7.02		.11	4.50
2600		.00	.25		.02	.03			2.18
2625			.05			.02		0.00	.30
2650			.00						0.03

Table IX (Cont.)

Fluxing Glass Content	A 30%	A 20%	A 10%	B 30%	B 20%	B 10%	C 30%	C 20%	C 10%	D 30%	D 20%	D 10%	E 30%	E 20%	E 10%	F 30%	F 20%	F 10%
Density (g/cc) vs. Firing Temperature (°F)																		
2350	2.32			2.40			2.41			2.33			2.29			2.45		
2375	2.32			2.42			2.43			2.34			2.31			2.44		
2400	2.34			2.42			2.43			2.25			2.34			2.44		
2425	2.35			2.42			2.43			2.23			2.34			2.45		
2450	2.36			2.25			2.37			1.99			2.38			2.41		
2475																		
2500	2.34			1.90			2.06			1.72			2.45			2.19		
2525		2.34			2.43			2.43			2.31			2.37			2.45	
2550		2.36			2.42			2.46			2.31			2.42			2.45	
2575		2.42			2.41			2.47			2.29			2.46			2.47	
2600		2.41	2.40		2.34	2.45		2.46	2.45		2.28	2.235		2.47	2.31		2.41	2.49
2625		2.38	2.40			2.45		2.32	2.46			2.35		2.48	2.37			2.49
2650			2.43			2.47			2.48			2.38			2.40			2.50
Moisture Absorption (%) vs. Firing Temperature (°F)																		
2350	.37			.10			.09			.11			.32			.04		
2375	.38			.05			.05			.02			.16			.03		
2400	.20			.03			.02			.03			.07			.02		
2425	.20			.03			.00			.01			.09			.00		
2450	.13			.03			.02			.05			.05			.03		
2475																		
2500	.04			.14			.10			.13			.05			.04		
2525		.13			.03			.01			.00			.06			.03	
2550		.08			.01			.01			.00			.02			.02	
2575		.08			.00			.01			.01			.05			.01	
2600		.16	.09		.17	.06		.02	.05		.01	.02		.10	.00		.04	.00
2625		.05	.12			.04		.08	.05			.04		.03	.10			.02
2650			.18			.04			.12			.03			.09			.03

Cb-98, Cb-96, Cb-910, C-A, C-B, C-C, C-D, C-E and C-F are shown in Table X. The

Table X

COEFFICIENT OF LINEAR THERMAL EXPANSION FOR

COMPOSITE BODIES AT 10%, 20% and 30% FLUXING GLASS

	Addition		
	10%	20%	30%
Cb-9	1.61*	1.83	2.07
Cb-98	1.65	1.75	1.94
Cb-96	1.44	1.61	1.77
Cb-910	1.59	1.67	1.83
C-A	1.55	1.68	1.73
C-B	1.37	1.57	1.89
C-C	1.64	1.75	1.81
C-D	1.59	1.86	2.11
C-E	1.53	1.54	1.73
C-F	1.55	1.73	1.91

*Times 10^{-6} in/in/°C

expansions are plotted in a $RO \cdot Al_2O_3 \cdot SiO_2$ ternary to show the effect of composition on thermal expansion; this is shown in Figs. 19 through 21.

As can be seen from the table, all compositions have quite low values for coefficients of linear thermal expansion. With a 10% addition, the values range from 1.37 x 10^{-6} for the C-B addition to 1.65 for the Cb-98 addition. For a 20% addition the values range from 1.61 x 10^{-6} for Cb-96 to 1.86 x 10^{-6} for C-D, and for the 30% additions, the values range from 1.73 x 10^{-6} for C-E up to 2.11 for C-D.

From a compositional standpoint, the 30% additions of glasses with the highest expansions (see Table VII and Fig. 18) generally produce the composite bodies with the highest expansions. With a 20% addition, this effect is still true, with the exception of C-B, but the difference in expansion with composition is not so well pronounced. With a 10% addition, the expansion of the cordierite predominates and all the expansions, with the exception of C-B and Cb-96, fall within a very narrow range.

iii. X-Ray Evaluation of Composite Bodies

An x-ray diffraction analysis of the composite bodies shows the presence of cordierite as the principal crystalline phase. Very minor amounts of other phases may be present, but they are not in sufficient quantity to be discernible from the background in the 10% and 20% bodies. Very minor peaks of BaC are found in the 30% bodies.

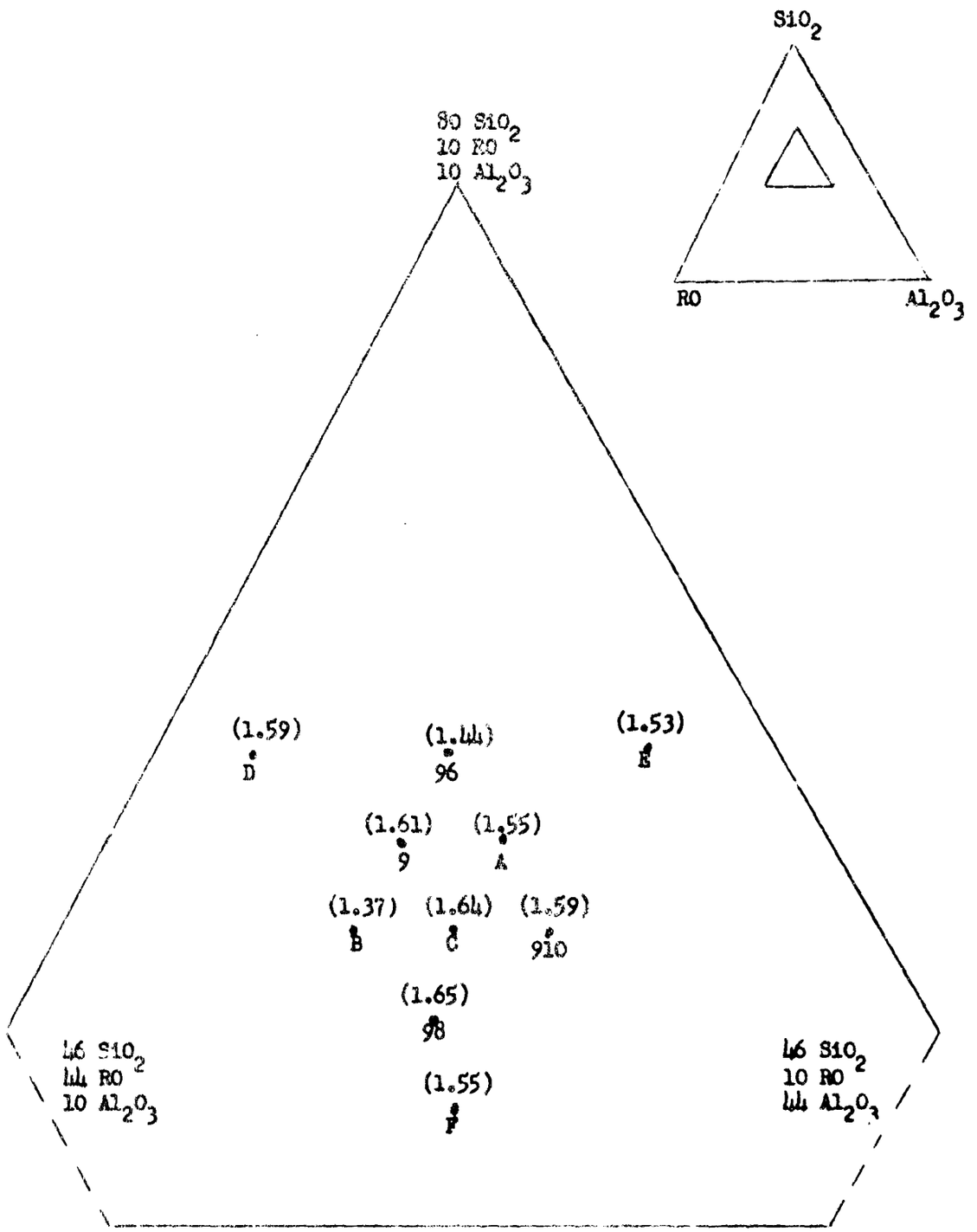

Fig. 19--Coefficients of Linear Thermal Expansion of Composite Bodies Studied in the $RO \cdot Al_2O_3 \cdot SiO_2$ System--10% Fluxing Glasses

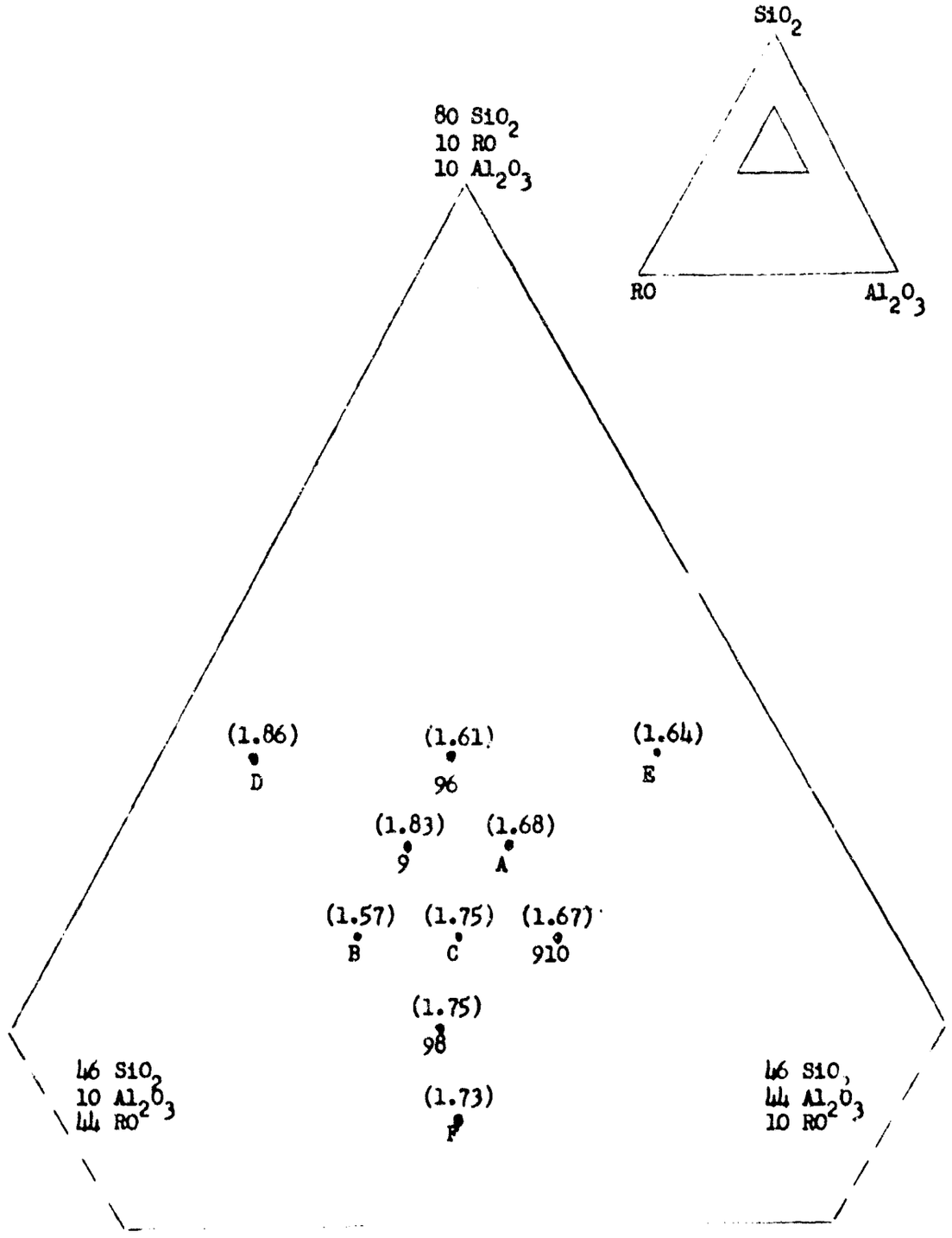

Fig. 20--Coefficients of Linear Thermal Expansion of Composite Bodies Studied in the $RO \cdot Al_2O_3 \cdot SiO_2$ System--20% Fluxing Glasses

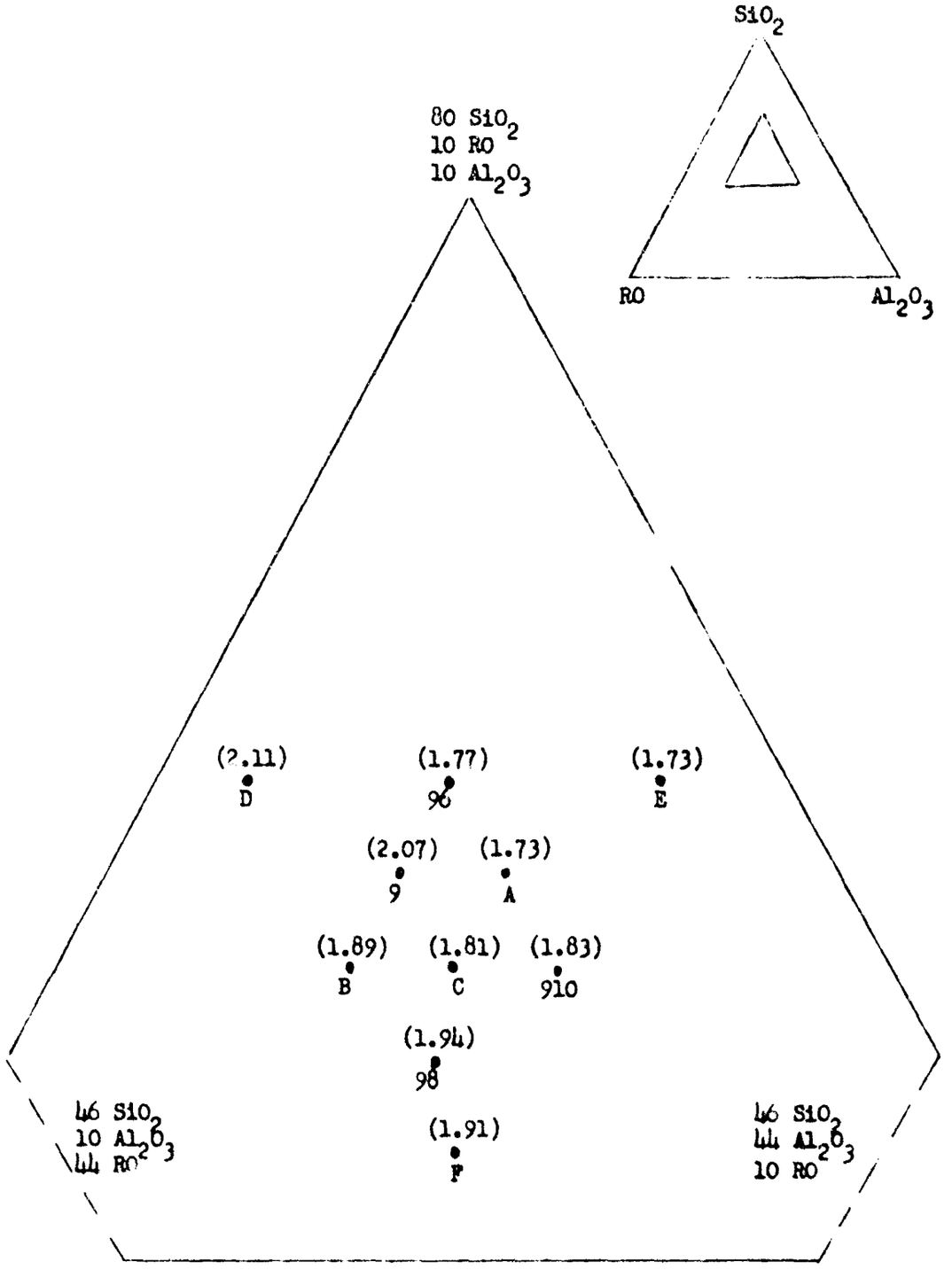

Fig. 21--Coefficients of Linear Thermal Expansion of Composite Bodies Studied in the $RO \cdot Al_2O_3 \cdot SiO_2$ System--30% Fluxing Glasses

F. Summary

This aspect of the research program dealt with the development of ceramic bodies which mature in the 1800-2600°F temperature range. The fabrication of these bodies has utilized the devitrification approach of the prereacted materials technique. This technique has been found to be superior to conventional fabrication from both physical and theoretical aspects.

The current research program dealt with the development of cordierite compositions exhibiting low thermal expansions and extended firing ranges. The problem was approached from two aspects. The first utilizes a raw material prepared by fritting the total composition; this is referred to as the one-frit approach. The second utilizes two frits, one of the theoretical cordierite composition and the other of a low melting, densifying glass in its fabrication; this is referred to as the two-frit approach.

In the study of the one-frit approach, 18 compositions were studied with regard to maturing properties and linear thermal expansion. Of these, two appeared promising, C-8 and C-13. These two compositions were further investigated for more complete detail with regard to their physical properties. It was found that these bodies possessed expansions as low as 1.69×10^{-6} in/in/°C, moderate transverse strength, 15,000 psi, and high values of the true density. They were further analyzed for crystalline phases present, microstructure, and electrical properties.

In the study of the two-frit approach, ten glasses were investigated as possible additive glasses to the cordierite glass. These glasses were evaluated individually with regard to maturing range, thermal expansion, crystalline phases which devitrify, and differential thermal analysis. All of these glasses lie within the $Al_2O_3 \cdot SiO_2 \cdot MgO \cdot CaO \cdot BaO$ system. Their thermal expansion ranged from 4.31 to 5.44×10^{-6} in/in/°C, with the value dependent entirely on the percentage of RO members present in the glass. These glasses were found to attain maturity as low as 1700°F and retain high density and maturation to 2250°F. Also, these glasses soften and devitrify into BaC plus an unknown phase at approximately the same temperature.

The densifying glasses were then added to a cordierite glass in amounts of 10, 20 and 30%. These bodies were evaluated with regard to linear thermal expansion, firing range, and x-ray analysis. It was found that the expansions varied from 1.37 to 1.65×10^{-6} in/in/°C for the 10% additions, from 1.57 to 1.86×10^{-6} in/in/°C for the 20% additions, and from 1.73 to 2.11×10^{-6} in/in/°C for the 30% additions. The firing range extended for 50°F with the 10% additions, 100°F for the 20% additions, and 150°F for the 30% additions. An x-ray analysis produced cordierite as the principal crystalline phase.

The results from both aspects of the study are quite promising. In each case, mature bodies, with reasonable firing ranges, were developed.

References

1. J. M. Stevels, "The Relation Between the Dielectric Losses and the Composition of Glass," J. of the Soc. of Glass Tech. (34), 80-100 (1950).
2. J. M. Stevels, J. Volger and C. van Amerengen, "The Dielectric Relaxation of Glass and the Pseudo-Capacity of Metal to Glass Interfaces, Measured at Extremely Low Frequencies," Philips Res. Reports (8), 452-470 (1953).
3. J. M. Stevels, "Some Experiments and Theories on the Power Factor of Glasses as a Function of their Composition II," Philips Res Reports (6), 34-53 (1951).
4. C. Kittle, Introduction to Solid State Physics (2d ed., J. Wiley & Sons, Inc., New York, 1960), p. 430-487.
5. N. N. Ault and F. H. McRitchie, "Design of a High Temperature Resistance Furnace," J. Am. Ceram. Soc. (33), 25-26 (1950).
6. N. N. Ault, personal correspondence.
7. Rn. N. McNally, F. I. Peters and P. H. Ribee, "Laboratory Furnace for Studies in Controlled Atmospheres; Melting Points of MgO in a N_2 Atmosphere and of Cr_2O_3 in H_2 and in Air Atmospheres," J. Am. Ceram. Soc. (44), 491-493 (1961).
8. J. Pappis and W. D. Kingery, "Electrical Properties of Single Crystal and Polycrystalline Alumina at High Temperatures," J. Am. Ceram. Soc. (44), 459-464 (1961).
9. J. Cohen, "Electrical Conductivity of Alumina," J. Am. Ceram. Soc. Bull. (38), 441-446 (1959).
10. P. J. Harrop and R. H. Creamer, "High Temperature Electrical Conduction of Single Crystal Alumina," Brit. J. Appl. Phys. (14), 335-339 (1963).
11. R. Chang, "Electrical Resistivity Changes of Alumina Crystal During Creep," J. Appl. Phys. (34), 1564-1565 (1963).
12. S. E. Keenle and F. M. Berting, "Electron Microscopy of Ceramics," Bell Labs. Record (34), 336-340 (1956).
13. I. Warshaw, "Structural Implications of the Electron Microscopy of Glass Surfaces," J. Am. Ceram. Soc. (43), 4-9 (1960).
14. J. J. Comer, "Electron Microscope Studies of Mullite Development in Fired Kaolinites,". J. Am. Ceram. Soc. (43), 378-384 (1960).
15. H. Pfisterer, E. Fuchs and W. Liesk, "Electron Microscopic Evidence of Ferroelectric Domains in Thin $BaTiO_3$ Single Crystal Films," Naturwissenschaften (49), 178-179 (1962).
16. P. E. Doherty and R. R. Leembrune, "Transmission Electron Microscopy of Glass-Ceramics," J. Am. Cer. Soc. (47), 368-370 (1964).
17. J. Washburn, A. Kelly and G. K. Williamson, "Electron Transmission Microscopy of Single Crystal Magnesium Oxide," Phil. Mag. (5), 192-193 (1960).
18. N. J. Tighe, "Jet Thinning Device for Preparation of Al_2O_3 Electron Microscope Specimens," Rev. of Scientific Inst. (35), 520-521 (1964).
19. M. Hirabayashi and S. Weissmann, "Study of CuAu I by Transmission Electron Microscopy," Acta Met. (10), 25-36 (1962).
20. N. J. Tighe and D. J. Barber, "Electron Microscopy and Diffraction of Synthetic Cerundum Crystals I, Pure Aluminum Oxide Grown by the Verneuil Process," Phil. Mag. (11), 495-512 (1965).
21. T. A. Verus, R. P. Jewett and O. E. Occountius, "Direct Observation of Dislocations in Sapphire," J. Am Ceram. Soc. (46), 459 (1963).
22. D. J. Barber, "Electron Microscopy and Difraction of Aluminum Oxide Whiskers," Phil. Mag. (10), 75-94 (1964).
23. J. Washburn, Electron Microscopy and Strength of Crystals (Interscience Publishers, New York, 1963), p. 301. 69, W. E. Elkington, G. Thomas and J. Washburn, "Damage Produced by Moving Dislocations in MgO," J. Am. Ceram. Soc. (46), 307-313 (196).

24. R. Scheuplein and P. Gibbs, "Surface Structure in Corundum--1, Etching of Dislocations," J. Am. Ceram. Soc. (43), 458-472 (1960).
25. V. D. Frechette, "Experimental Techniques for Microstructure Investigation," Microstructure of Ceramic Materials (Proceedings of an American Ceramic Society Symposium, Pittsburgh, Pa., April 27-28, 1963. U. S. Dept. Commerce, National Bureau of Standards, Miscellaneous Publication 257).
26. R. C. McVickers, S. D. Ford and R. A. Dugdale, "Polishing and Etching Techniques for Dense Alumina," J. Am. Ceram. Soc. (45), 199 (1962).
27. W. J. Alford and D. L. Stevens, "Chemical Polishing and Etching Techniques of Al_2O_3 Single Crystals," J. Am. Ceram. Soc., (46), 193-194 (1963).
28. B. D. Cullity, Elements of X-Ray Diffraction (Addison-Wesley Publishing Co., Inc., Reading, Mass., 1959), p. 42, pp. 149-176.
29. P. J. Jorgensen and J. H. Westbrook, "Role of Solute Segregation at Grain Boundaries during Final Stage Sintering of Alumina," J. Am. Ceram. Soc. (47), 332-338 (1964).
30. D. M. Keffman, "Application of the Electron Probe to the Determination of Concentration Gradients and Dispersed Phase Compositions," Norelco Reporter (11), 59-61 (1964).
31. S. H. Moll, "Some Applications of the Electron Probe Microanalyzer," Norelco Reporter (11), 55-58 (1964).
32. Discussion and experimental assistance of Mr. J. Zitterman and Mr. W. Whitney of Corning Glass Works.
33. B. J. Wuensch and T. Vasiloz, "Grain Boundary Diffusion in MgO," J. Am. Ceram. Soc. (47), 63-68 (1964).
34. P. J. Jorgensen, "Modification of Sintering Kinetics by Solute Segregation in Al_2O_3," J. Am. Ceram Soc. (48), 207-211 (1965).
35. C. A. Bruch, "Sintering Kinetics for the High Density Alumina Process," J. Am. Ceram. Soc. Bull. (41), 799-806 (1962).
36. R. L. Coble, "Sintering Crystalline Solids," Part I and II," J. Appl. Phys. (32), 787-799 (1961).
37. D. L. Johnson and I. B. Cutler, "Diffusion Sintering I. Initial Stage Sintering Models and Their Application to Shrinkage of Powder Compacts," J. Am. Ceram. Soc. (46), 541-545 (1963). "Initial Sintering Kinetics of Alumina," ibid., 545-550.
38. L. Navias, "Preparation and Properties of Spinel Made by Vapor Transport and Diffusion in the System $MgO-Al_2O_3$," J. Am. Ceram. Soc. (44), 434-446 (1961).
39. Discussion and experimental assistance of Dr. W. C. Allen, Rutgers University, New Brunswick, New Jersey.

UNCLASSIFIED
Security Classification

DOCUMENT CONTROL DATA - R&D

(Security classification of title, body of abstract and indexing annotation must be entered when the overall report is classified)

1 ORIGINATING ACTIVITY (Corporate author) Rutgers - The State University New Brunswick, New Jersey 08903	2a REPORT SECURITY CLASSIFICATION 2b GROUP

3 REPORT TITLE

STUDIES OF CERAMIC PROCESSING

4 DESCRIPTIVE NOTES (Type of report and inclusive dates)

Final; December 1, 1964, to December 15, 1965

5 AUTHOR(S) (Last name, first name, initial)

Smoke, E. J., Rinfel, C. M., and Fleischner, P. L.

6 REPORT DATE	7a TOTAL NO OF PAGES	7b NO OF REFS
December 1, 1964, to December 15, 1965	73	39

8a CONTRACT OR GRANT NO NOw 65-0199-d b PROJECT NO c d	9a ORIGINATOR'S REPORT NUMBER(S) 9b OTHER REPORT NO(S) (Any other numbers that may be assigned this report)

10 AVAILABILITY/LIMITATION NOTICES

Distribution of this document is unlimited.

11 SUPPLEMENTARY NOTES	12 SPONSORING MILITARY ACTIVITY
	U. S. Navy, Bureau of Weapons

13 ABSTRACT

The objective of this program is to improve the structure of ceramics by processing. The over-all temperature range of interest is 1800 to above 3000°F. In the high portion of the range, 3000°F and above, compositions of pure alumina plus 0 to 2% additions of MgO were studied between 2822 and 3150°F, at 1 to 7 hour soaking periods and in atmospheres of hydrogen, helium and vacuum. This work was reported in the previous Final Report; however, the analysis of results is reported herein. Petrographic, x-ray, d.c. conductivity, electron transmission and electron probe methods were used and the results are reported. The second temperature range, 2600-3000°F, was studied utilizing the presintered approach to the prereacted raw materials technique and the results were reported in earlier reports. The low range, 1800 to 2600°F, was studied using the devitrification approach to the prereacted materials technique. The area of crystallization of cordierite in the $MgO \cdot Al_2O_3 \cdot SiO_2$ system was evaluated as a single glass sytem. A two-glass system, in which one glass devitrifies cordierite and the second supplies the bonding system, was studied. Bonding glass compositions were evaluated in the $RO \cdot Al_2O_3 \cdot SiO_2$ system, in which the RO members are alkaline earth oxides. Composites were made at 10, 20 and 30% bonding glass. Processing, structures and properties are reported.

DD FORM 1473

UNCLASSIFIED
Security Classification

UNCLASSIFIED

Security Classification

14 KEY WORDS	LINK A		LINK B		LINK C	
	ROLE	WT	ROLE	WT	ROLE	WT
sinter						
prereaction						
devitrification						
presintering						
structure						
composite						
cordierite						
alumina						
bonding glass						
fluxing						

INSTRUCTIONS

1. ORIGINATING ACTIVITY: Enter the name and address of the contractor, subcontractor, grantee, Department of Defense activity or other organization *(corporate author)* issuing the report.

2a. REPORT SECURITY CLASSIFICATION: Enter the overall security classification of the report. Indicate whether "Restricted Data" is included. Marking is to be in accordance with appropriate security regulations.

2b. GROUP: Automatic downgrading is specified in DoD Directive 5200.10 and Armed Forces Industrial Manual. Enter the group number. Also, when applicable, show that optional markings have been used for Group 3 and Group 4 as authorized.

3. REPORT TITLE: Enter the complete report title in all capital letters. Titles in all cases should be unclassified. If a meaningful title cannot be selected without classification, show title classification in all capitals in parenthesis immediately following the title.

4. DESCRIPTIVE NOTES: If appropriate, enter the type of report, e.g., interim, progress, summary, annual, or final. Give the inclusive dates when a specific reporting period is covered.

5. AUTHOR(S): Enter the name(s) of author(s) as shown on or in the report. Enter last name, first name, middle initial. If military, show rank and branch of service. The name of the principal author is an absolute minimum requirement.

6. REPORT DATE: Enter the date of the report as day, month, year, or month, year. If more than one date appears on the report, use date of publication.

7a. TOTAL NUMBER OF PAGES: The total page count should follow normal pagination procedures, i.e., enter the number of pages containing information.

7b. NUMBER OF REFERENCES: Enter the total number of references cited in the report.

8a. CONTRACT OR GRANT NUMBER: If appropriate, enter the applicable number of the contract or grant under which the report was written.

8b, 8c, & 8d. PROJECT NUMBER: Enter the appropriate military department identification, such as project number, subproject number, system numbers, task number, etc.

9a. ORIGINATOR'S REPORT NUMBER(S): Enter the official report number by which the document will be identified and controlled by the originating activity. This number must be unique to this report.

9b. OTHER REPORT NUMBER(S): If the report has been assigned any other report numbers *(either by the originator or by the sponsor)*, also enter this number(s).

10. AVAILABILITY/LIMITATION NOTICES: Enter any limitations on further dissemination of the report, other than those imposed by security classification, using standard statements such as:

(1) "Qualified requesters may obtain copies of this report from DDC."

(2) "Foreign announcement and dissemination of this report by DDC is not authorized."

(3) "U. S. Government agencies may obtain copies of this report directly from DDC. Other qualified DDC users shall request through

_____."

(4) "U. S. military agencies may obtain copies of this report directly from DDC. Other qualified users shall request through

_____."

(5) "All distribution of this report is controlled. Qualified DDC users shall request through

_____."

If the report has been furnished to the Office of Technical Services, Department of Commerce, for sale to the public, indicate this fact and enter the price, if known.

11. SUPPLEMENTARY NOTES: Use for additional explanatory notes.

12. SPONSORING MILITARY ACTIVITY: Enter the name of the departmental project office or laboratory sponsoring *(paying for)* the research and development. Include address.

13. ABSTRACT: Enter an abstract giving a brief and factual summary of the document indicative of the report, even though it may also appear elsewhere in the body of the technical report. If additional space is required, a continuation sheet shall be attached.

It is highly desirable that the abstract of classified reports be unclassified. Each paragraph of the abstract shall end with an indication of the military security classification of the information in the paragraph, represented as *(TS), (S), (C), or (U)*

There is no limitation on the length of the abstract. However, the suggested length is from 150 to 225 words.

14. KEY WORDS: Key words are technically meaningful terms or short phrases that characterize a report and may be used as index entries for cataloging the report. Key words must be selected so that no security classification is required. Identifiers, such as equipment model designation, trade name, military project code name, geographic location, may be used as key words but will be followed by an indication of technical context. The assignment of links, rules, and weights is optional.

UNCLASSIFIED

Security Classification